

A new class of SUSY signatures in the processes $gg \rightarrow HH', VH.$

G.J. Gounaris^a, J. Layssac^b, and F.M. Renard^b

^aDepartment of Theoretical Physics, Aristotle University of Thessaloniki,
Gr-54124, Thessaloniki, Greece.

^bLaboratoire de Physique Théorique et Astroparticules, UMR 5207
Université Montpellier II, F-34095 Montpellier Cedex 5.

Abstract

Within the MSSM and SM frameworks, we analyze the 1loop electroweak (EW) predictions for the helicity amplitudes describing the 17 processes $gg \rightarrow HH'$, and the 9 processes $gg \rightarrow VH$; where H, H' denote Higgs or Goldstone bosons, while $V = Z, W^\pm$. Concentrating on MSSM, we then investigate how the asymptotic helicity conservation (HCns) property of SUSY, affects the amplitudes at the LHC energy range; and what is the corresponding situation in SM, where no HCns theorem exists. HCns is subsequently used to construct many relations among the cross sections of the above MSSM processes, depending only on the standard MSSM angles α and β characterizing the two Higgs doublets. These relations should be asymptotically exact; but as the energy decreases towards the LHC range, mass-depending deviations should start appearing. Provided the SUSY scale is not too high, these relations may remain roughly correct, even at the LHC energy range.

PACS numbers: 12.15.-y, 12.15.-Lk, 14.70.Fm, 14.80.Ly

1 Introduction

The fact that Supersymmetry confers remarkable properties to scattering amplitudes at high energy, has already been noticed in the literature. One aspect of it emphasized some time ago, is that in processes involving standard external particles and non-vanishing Born contributions, the coefficients of the 1loop linear logarithmic corrections at high energy differ strikingly, between the minimal supersymmetric model (MSSM) and the standard model (SM), reflecting the differences in the gauge and Yukawa interactions [1, 2, 3].

Another aspect concerns the important helicity conservation (HCns) theorem established in supersymmetry (SUSY) [4]. This property demands that for any 2-to-2 process, all amplitudes that violate HCns, exactly vanish, at energies much higher than all masses, and fixed angles. More explicitly this theorem states that for any process

$$a_{\lambda_a} + b_{\lambda_b} \rightarrow c_{\lambda_c} + d_{\lambda_d} \quad , \quad (1)$$

with λ_j denoting the particle helicity, all amplitudes satisfying

$$\lambda_a + \lambda_b - \lambda_c - \lambda_d \neq 0 \quad , \quad (2)$$

vanish exactly at asymptotic energies. The amplitudes obeying (2), are called below helicity violating (HV) amplitudes; while those satisfying $\lambda_a + \lambda_b - \lambda_c - \lambda_d = 0$, are termed as helicity conserving (HC) amplitudes. HCns should be true to all orders in the SUSY couplings, drastically reducing the number of the asymptotically non-vanishing amplitudes [4].

This HCns theorem is particularly non-trivial for processes involving external gauge bosons, where huge cancelations among the various diagrams conspire for its realization [4]. Moreover, the theorem crucially depends on the renormalizability of the model; any anomalous coupling will violate it [5].

In SM there is no general all-order proof for HCns. Nevertheless, in several processes, it has been found to be approximately correct. Thus, if the Born contribution is non-vanishing, then at the tree level, the HV amplitudes for any 2-to-2 processes always vanish asymptotically, while the HC ones tend to usually non vanishing constants [4]. If 1loop corrections are included to such processes, then HCns remains approximately correct; in the sense that the HC amplitudes receive considerable \ln - and \ln^2 -corrections at high energies, and are always much larger than the HV amplitudes, which however do not necessarily vanish asymptotically [1].

Concerning processes with vanishing Born contributions, we mention $\gamma\gamma \rightarrow ZZ$, γZ , $\gamma\gamma$, studied some time ago, at the complete 1loop EW order, in both SM and MSSM [6]. In these cases, it has then been seen explicitly in both, SM and MSSM, that the HC amplitudes rise logarithmically, due to the gauge (and gaugino in MSSM) loop contributions, and are predominantly imaginary [6]. On the contrary, the HV amplitudes tend to angle-dependent small constants in SM, but vanish in MSSM [6].

Thus, in all SM cases studied so far, HCns is approximately valid; in the sense that the HC amplitudes dominate the HV ones, but the HV amplitudes do not necessarily vanish

asymptotically. For SM processes with vanishing Born contributions though, no general statement on, even the approximate validity of HCns exists in the literature.

Coming back to the supersymmetric case, where HCns has been proved to all orders for asymptotic energies [4]; we remark that its relevance for realistic energies is process-dependent and needs to be separately investigated.

To this aim, the complete 1loop electroweak (EW) corrections were calculated for $ug \rightarrow dW^+$, which determines W +jet production at LHC [7]. Assuming that the SUSY masses are in the range set by the $SPS1a'$ benchmark of the SPA convention¹ [8], it has been found that the HC amplitudes are much larger than the HV ones, for energies $\gtrsim 0.5$ TeV, and a wide range of angles [7]. Similar results are expected for benchmarks with somewhat heavier SUSY masses, like those in Table 1.

Table 1: Input parameters at the grand scale, for three constrained MSSM benchmark models with $\mu > 0$; dimensional parameters in GeV.

	$SPS1a'$ [8]	BBSSW [10]	FLN mSP4 [11]
$m_{1/2}$	250	900	137
m_0	70	4716	1674
A_0	-300	0	1985
$\tan \beta$	10	30	18.6

Furthermore, to the 1loop EW order in MSSM, HCns was used to derive relations between the differential cross sections for the subprocess $ug \rightarrow dW^+$ and $ug \rightarrow \tilde{d}_L \tilde{\chi}_i^+$, where \tilde{d}_L denotes an L-down-squark and $\tilde{\chi}_i^+$ describes any of the two charginos [12]. The derivation of these relations was based on the asymptotic properties of the helicity amplitudes. But for benchmarks like those in Table 1, the relations remained approximately correct, even at LHC energies; where the HCns validity for the $ug \rightarrow \tilde{d}_L \tilde{\chi}_i^+$ amplitudes, is not yet reached [12]. Similar relations should be true for many other analogous pairs of processes.

In the present work we propose to study more stringently the helicity conservation property; i.e. to study the energies needed for establishing HCns in MSSM, and possibly identify cases where it is strongly violated in SM.

We therefore look at processes where the dominant HC amplitudes do not increase logarithmically at high energies, but rather tend to angular dependent, "constants". Our previous experience implies that in such cases there should be no Born contribution [1]; and moreover, that there should not be any gauge exchange contributions, like those in $\gamma\gamma \rightarrow ZZ, \gamma Z, \gamma\gamma$ [6].

In the MSSM case, where HCns is obeyed, we could then also derive asymptotic relations analogous to those in [12]; hoping that they may again be useful, even at the LHC range.

¹This model is very close to the best fit of the precision data in [9].

Thus, we study here the gluon-gluon fusion to gauge or Higgs bosons, at the complete 1loop EW order, in either SM or MSSM. For simplicity, we assume a CP invariant framework, where all soft breaking terms and superpotential and Yukawa couplings are real. More explicitly the processes we study are

$$g(l, \mu)g(l', \mu') \rightarrow H(p)H'(p') \quad , \quad g(l, \mu)g(l', \mu') \rightarrow V(p, \tau)H(p') \quad , \quad (3)$$

where

$$H, H' \Rightarrow H^\pm, G^\pm, H_{SM}, H^0, h^0, G^0, A^0 \quad , \quad (4)$$

denote the Higgs or Goldstone bosons in MSSM or SM , and²

$$V \Rightarrow W^\pm, Z \quad . \quad (5)$$

In (3), (μ, μ', τ) describe the helicities of the two incoming gluons and the final vector boson respectively, while (l, l') are the incoming momenta, and (p, p') the outgoing.

Concerning $gg \rightarrow HH'$, we consider the 17 processes

$$\begin{aligned} 4 \text{ SM processes} &\rightarrow HH, G^0H, G^+G^-, G^0G^0, \\ 13 \text{ MSSM processes} &\rightarrow H^+H^-, H^0H^0, h^0h^0, H^0h^0, A^0h^0, A^0H^0, A^0A^0, \\ &G^0h^0, G^0H^0, G^+H^-, G^0A^0, G^+G^-, G^0G^0, \end{aligned} \quad (6)$$

calculated from the general graphs of Fig.1. For each of these process, we study the energy and angular behaviour of the four helicity amplitudes corresponding to $\mu = \pm 1$ and $\mu' = \pm 1$, emphasizing the difference between the HC and HV amplitudes.

Turning next to $gg \rightarrow VH$, we consider the 9 processes

$$\begin{aligned} 3 \text{ SM processes} &\rightarrow ZH, W^+G^-, ZG^0, \\ 6 \text{ MSSM processes} &\rightarrow W^+H^-, ZH^0, Zh^0, ZA^0, W^+G^-, ZG^0, \end{aligned} \quad (7)$$

calculated from the diagrams in Fig.2. In these cases, we have a richer helicity structure with $\mu = \pm 1$, $\mu' = \pm 1$ and $\tau = \pm 1, 0$.

FORTTRAN codes calculating the helicity amplitudes for all these processes are constructed, which are released in [13].

We indeed find that the HC amplitudes dominate at high energies in MSSM, behaving like angular dependent "constants", for both groups of processes in (6) and (7). Several relations among the dominant HC amplitudes for such processes are established. These are used to derive asymptotic relations among various cross sections, which may lead to interesting tests of the underlying supersymmetric structure, even at non-asymptotic energies.

In SM, the HC amplitudes of (3) are again found to behave asymptotically like angular dependent "constants". But the HCns picture is distorted, and some helicity violating

² $V = \gamma$ is impossible due to CP invariance.

(HV) amplitudes also tend to "constants", comparable in magnitude to those of the HC ones. There exist processes though, where in SM also, the HV amplitudes vanish at high energies.

Cross sections for the 1loop EW contributions to many such processes exist in the literature [14, 15, 16, 17, 18]; but a detail amplitude analysis studying the helicity conservation property, has not yet been done.

The contents of the paper are: In Section 2 we present the general structure of the $gg \rightarrow HH'$ and $gg \rightarrow VH$ amplitudes. In Section 3, the high energy behaviours of the helicity amplitudes for the various processes, are analyzed; and the asymptotic relations among several cross sections are derived. In Section 4, we introduce the aforementioned FORTRAN codes, which calculate the 1loop EW helicity amplitude; and we give our numerical results. Particular attention is payed towards investigating the behaviour of the above asymptotic cross section relations, as the energy decreases. Finally, Section 5 contains the summary and an outlook.

We do not make any detail proposal for an LHC observable, in this paper. Applications to LHC would require additional work including QED and (most importantly) QCD corrections [19], as well as the final state identification and background analysis, which are beyond the scope of this paper.

2 The $gg \rightarrow HH'$ and $gg \rightarrow VH$ amplitudes

The $gg \rightarrow HH'$ case.

Defining the kinematics for the process $gg \rightarrow HH'$ as in (3), the corresponding helicity amplitudes are written as $F_{\mu\mu'}^{HH'}(s, \theta)$, where s is the square of the c.m. energy, and θ is the corresponding scattering angle; ($0 < \theta < \pi$). A color factor δ^{ab} has always been removed from the amplitudes, where (a, b) describe the color indices of the two incoming gluons. The phase of $F_{\mu\mu'}(s, \theta)$, is related to the phase of the S -matrix by $S = iF\delta^{ab}$.

Bose statistics for the initial gluons and CP invariance imply

$$\begin{aligned}
\text{Bose} &\Rightarrow F_{\mu\mu'}(\theta) = F_{\mu'\mu}(\pi - \theta) \quad , \\
\text{CP} &\Rightarrow F_{\mu\mu'}^{H_a^0 H_{a'}^0}(\theta) = F_{-\mu-\mu'}^{H_a^0 H_{a'}^0}(\theta) \quad , \quad F_{\mu\mu'}^{H_b^0 H_{b'}^0}(\theta) = F_{-\mu-\mu'}^{H_b^0 H_{b'}^0}(\theta) \quad , \\
&F_{\mu\mu'}^{H_a^0 H_b^0}(\theta) = -F_{-\mu-\mu'}^{H_a^0 H_b^0}(\theta) \quad , \\
&F_{\mu\mu'}^{H^\pm H^\mp}(\theta) = F_{-\mu-\mu'}^{H^\mp H^\pm}(\theta) \quad ,
\end{aligned} \tag{8}$$

where the charged final state relations also apply for the $H^\pm G^\mp$ and $G^\pm G^\mp$ amplitudes. In MSSM we use the notation $H_a^0 = (H^0, h^0)$ and $H_b^0 = (A^0, G^0)$, while in SM we identify $H_a^0 = H$ and $H_b^0 = G^0$.

Relations (8) constrain the four $gg \rightarrow HH'$ amplitudes

$$F_{++}, F_{+-}, F_{-+}, F_{--} \quad , \tag{9}$$

so that the first two may be considered as independent. According to HCns, only $F_{\pm\mp}$ survive asymptotically in MSSM [4]. The corresponding cross section is

$$\frac{d\sigma(gg \rightarrow HH')}{d \cos \theta} = \frac{|\vec{p}|}{512\pi s\sqrt{s}} \sum_{\mu,\mu'} |F_{\mu\mu'}|^2, \quad (10)$$

where the summation is over all possible ($\mu = \pm 1$, $\mu' = \pm 1$), and $|\vec{p}|$ denotes the absolute value of the 3-momentum in the c.m. of the HH' pair.

The generic set of the 1loop EW diagrams for $gg \rightarrow HH'$ in MSSM and SM is presented in Fig.1, where full, broken and wavy lines describe respectively fermionic, scalar and vector particles. The contributions from interchanging the two gluons should be added for the diagrams³ $A, A', B, B', B'', F, G, H, J$; on the contrary, for the diagrams C, C', C'', D , the gluon-symmetrization is automatically included.

No (H, H') symmetrization is assumed. Consequently, for the F and G boxes, the respective quark- and squark-loops are independent of the corresponding antiquark- and antisquark-loops, which should therefore be added respectively. For the rest of the graphs, only the quark or squark loops are needed.

The specific graphs of Fig.1 contributing to each of the 17 processes in (6), are

- In SM, the only relevant boxes are F and H, which contribute to all possible processes in (6).

In MSSM, all F, G, H, J boxes contribute to the processes in (6).

- Triangle and bubble contributions in SM arise as follows:
 - for $gg \rightarrow HH$, G^0G^0 , they come from graph A with $H'' = H$;
 - for $gg \rightarrow G^0H$, they come from graph A with $H'' = G^0$, and graph A' with $V = Z$;
 - for $gg \rightarrow G^+G^-$, they come from graph A with $H'' = H$.
- Triangle and bubble contributions in MSSM arise as follows:
 - for $gg \rightarrow H^0H^0$, h^0h^0 , H^0h^0 , A^0A^0 , G^0G^0 , A^0G^0 , they come from graphs A, B, C , with $H'' = H^0, h^0$; and from graphs B'', C'', D ;
 - for $gg \rightarrow A^0H^0$, A^0h^0, G^0H^0 , G^0h^0 , they come from graph A with ($H'' = A^0, G^0$); and graphs A', B', C' with $V = Z$;
 - for $gg \rightarrow H^+H^-, G^+G^-$, they come from graphs A, B, C , with ($H'' = H^0, h^0$); and from graphs B'', C'', D ;
 - for $gg \rightarrow G^+H^-$, they come from graph A with ($H'' = H^0, h^0, A^0$); from graphs B, C , with ($H'' = H^0, h^0$); and from graphs B'', C'', D .

³The diagram-names are indicated in Fig.1, as well as the definitions of H'' and V used below.

The $gg \rightarrow VH$ amplitudes.

Using again the notation (3), we describe the helicity amplitudes as $F_{\mu\mu'\tau}^{VH}(s, \theta)$. The same phase conventions as in the previous subsection are used, and a color factor δ^{ab} is again removed.

Bose statistics for the initial gluons and CP invariance imply

$$\begin{aligned}
\text{Bose} &\Rightarrow F_{\mu\mu'\tau}(\theta) = (-1)^\tau F_{\mu'\mu\tau}(\pi - \theta) \quad , \\
\text{CP} &\Rightarrow F_{\mu\mu'\tau}^{ZH_a^0}(\theta) = (-1)^{(1-\tau)} F_{-\mu-\mu'-\tau}^{ZH_a^0}(\theta) \quad , \\
&\Rightarrow F_{\mu\mu'\tau}^{ZH_b^0}(\theta) = -(-1)^{(1-\tau)} F_{-\mu-\mu'-\tau}^{ZH_b^0}(\theta) \quad , \\
&\Rightarrow F_{\mu\mu'\tau}^{W^+H^-}(\theta) = (-1)^{(1-\tau)} F_{-\mu-\mu'-\tau}^{W^-H^+}(\theta) \quad , \\
&F_{\mu\mu'\tau}^{W^+G^-}(\theta) = (-1)^{(1-\tau)} F_{-\mu-\mu'-\tau}^{W^-G^+}(\theta) \quad ,
\end{aligned} \tag{11}$$

where H_a^0, H_b^0 are defined immediately after (8).

Relations (11) constrain the 12 possible helicity amplitudes

$$\begin{aligned}
&F_{+++} \quad , \quad F_{++-} \quad , \quad F_{++0} \quad , \quad F_{+-+} \quad , \quad F_{+--} \quad , \quad F_{+-0} \quad , \\
&F_{---} \quad , \quad F_{--0} \quad , \quad F_{--+} \quad , \quad F_{-++} \quad , \quad F_{-+-} \quad , \quad F_{-+0} \quad ,
\end{aligned} \tag{12}$$

so that the first six may be considered as the independent for neutral final states, while for charged final states we take the first nine as independent. According to the HCNs theorem, only $F_{\pm\mp 0}$ may survive at asymptotic energies in MSSM [4]. The corresponding cross section is given by

$$\frac{d\sigma(gg \rightarrow VH)}{d\cos\theta} = \frac{|\vec{p}|}{512\pi s\sqrt{s}} \sum_{\mu, \mu', \tau} |F_{\mu\mu'\tau}|^2 \quad , \tag{13}$$

where the summation is done over all possible ($\mu = \pm 1, \mu' = \pm 1$) and ($\tau = \pm 1, 0$). In (13), $|\vec{p}|$ denotes the absolute value of the 3-momentum in the c.m. of the final VH pair.

The generic set of the 1loop EW diagrams for $gg \rightarrow VH$ in MSSM and SM is presented in Fig.2; where full, broken and wavy lines again describe respectively the fermionic, scalar and vector particles. As before, the contributions from interchanging the two gluons should be added for the diagrams⁴ $A, A', B, B', E, F, G, H, J$; while for C, C', D , the gluon-symmetrization is automatically included. For the F and G boxes we should add to the respective quark- and squark-loop contributions, the corresponding antiquark- and antisquark-loops. For the rest of the graphs, only the quark or squark loops are needed.

The specific graphs of Fig.2 contributing to each of the 9 processes in (7), are⁵:

- In SM, the relevant boxes F and H contribute to all processes in (7).

In MSSM, all F, G, H, J boxes contribute to the processes in (7).

⁴The names of the diagrams are defined in Fig.2.

⁵The definitions of H' and V' for the items below are given in Fig.2.

- Triangle and bubble contributions in SM appear as follows:
 - for $gg \rightarrow ZH$, they come from graph A with $H' = G^0$, and from graph A' with $V' = Z$;
 - for $gg \rightarrow ZG^0$, they come from graph A with $H' = H$;
 - for $gg \rightarrow W^+G^-$, they come from graph A with $(H' = H, G^0)$, and from graph A' with $(V' = \gamma, Z)$.
- Triangle and bubble contributions in MSSM appear as follows:
 - for $gg \rightarrow ZH^0, Zh^0$, they come from graph A with $(H' = A^0, G^0)$, and from graphs A', B', C' with $V' = Z$;
 - for $gg \rightarrow ZA^0, ZG^0$, they come from graphs A, B, C with $(H' = h^0, H^0)$;
 - for $gg \rightarrow W^+H^-$, they come from graph A with $(H' = h^0, H^0, A^0)$, from graphs B, C with $(H' = h^0, H^0)$, and from graphs D, E ;
 - for $gg \rightarrow W^+G^-$, they come from graph A with $(H' = h^0, H^0, G^0)$, from graphs B, C with $(H' = h^0, H^0)$, from graphs A', B', C' with $(V' = \gamma, Z)$, and from graphs D, E .

Finally we note that the processes in (6,7) which involve final Goldstone bosons, provide a useful test of the validity of our calculations at high energies. This comes from the equivalence theorem which states that at high energies we should have [22]

$$\begin{aligned}
 F_{\mu\mu'0}(gg \rightarrow W^\pm H^\mp) &\simeq \mp \xi_W F_{\mu\mu'}(gg \rightarrow G^\pm H^\mp) , \\
 -iF_{\mu\mu'0}(gg \rightarrow ZH_{a,b}^0) &\simeq \xi_Z F_{\mu\mu'}(gg \rightarrow G^0 H_{a,b}^0) .
 \end{aligned}
 \tag{14}$$

We have checked that these relations are satisfied by the results of our codes, where $\xi_W = \xi_Z = 1$ is always used.

Similarly, the processes in (6) involving two final Goldstones, determine the high energy behavior of $gg \rightarrow V_1 V_2$, for two longitudinal vector bosons [22].

3 High energy properties

3.1 Analytical results for $gg \rightarrow HH'$ in MSSM

The high energy behaviour of the amplitudes for the $gg \rightarrow HH'$ processes in (6), may be analytically obtained from the diagrams in Fig.1 and the asymptotic expressions given e.g. in [23].

The only diagrams of Fig.1, which are not suppressed at high energies, are B'' , C'' , F , H . Considered separately, the B'' and C'' contributions go to constants; while the F and H boxes have linear $\ln(s)$ behaviours, which cancel out in their sum. Thus, the complete contribution behaves like an angle-dependent, but energy independent "constant", for all $gg \rightarrow HH'$ processes. Subtleties arise in specific processes though, depending on the relative importance of these diagrams.

Thus, in SM, where the squark diagrams are absent, the available processes HH , G^0G^0 , G^0H , G^+G^- receive their complete asymptotic "constant" contribution solely from the F and H boxes.

For MSSM, we first concentrate on the G^0G^0 and G^+G^- processes, where the constants from the $F + H$ boxes are canceled in $F_{\pm\pm}$, by opposite constants coming from the squark diagrams (B'' , C''), leaving mass-suppressed contributions that vanish at high energies and fixed angles. Only the HC amplitudes $F_{\pm\mp}$ survive asymptotically, characterized by energy independent, but angle dependent "constants". Similar situations arise also for all other MSSM processes, in agreement with HCns [4].

To describe in more detail the HC asymptotic amplitudes, it is convenient to divide these MSSM processes into three classes, as follows:

- Class a: It contains the 6 processes (k=1,6)

$$G^0G^0, G^0A^0, A^0A^0, H^0H^0, h^0h^0, H^0h^0,$$

characterized by neutral final bosons carrying identical CP eigenvalues. The corresponding asymptotic limits for $F_{\pm\mp}^k$ may then be expressed as⁶

$$\begin{aligned} F_{\pm\mp}^k &\rightarrow R_{ak} C_{\pm\mp}^I(\theta), \quad \text{with} \\ R_{a1} &= m_t^2 + m_b^2, \\ R_{a2} &= m_t^2 \cot \beta - m_b^2 \tan \beta, \\ R_{a3} &= m_t^2 \cot^2 \beta + m_b^2 \tan^2 \beta, \\ R_{a4} &= \frac{m_t^2 \sin^2 \alpha}{\sin^2 \beta} + \frac{m_b^2 \cos^2 \alpha}{\cos^2 \beta}, \\ R_{a5} &= \frac{m_t^2 \cos^2 \alpha}{\sin^2 \beta} + \frac{m_b^2 \sin^2 \alpha}{\cos^2 \beta}, \\ R_{a6} &= \frac{m_t^2 \sin \alpha \cos \alpha}{\sin^2 \beta} - \frac{m_b^2 \cos \alpha \sin \alpha}{\cos^2 \beta}, \end{aligned} \tag{15}$$

where $C_{\pm\mp}^I(\theta)$ describe the process-independent part of these limits, while the real quantities R_{ak} describe the process-dependent part. The later solely depend on the MSSM angles α , (describing the standard two-Higgs-doublet mixing angle), and β (related to the ratio of the Higgs vacuum expectation values) [24].

⁶We use the same conventions as in [24].

- Class b: It contains the 4 processes (k=1,4)

$$G^0 H^0 , G^0 h^0 , A^0 H^0 , A^0 h^0 ,$$

characterized by neutral final bosons carrying opposite CP eigenvalues. The corresponding asymptotic limits for $F_{\pm\mp}^k$ then become

$$\begin{aligned} F_{\pm\mp}^k &\rightarrow R_{bk} C_{\pm\mp}^J(\theta) , \quad \text{with} \\ R_{b1} &= \frac{m_t^2 \sin \alpha}{\sin \beta} - \frac{m_b^2 \cos \alpha}{\cos \beta} , \\ R_{b2} &= \frac{m_t^2 \cos \alpha}{\sin \beta} + \frac{m_b^2 \sin \alpha}{\cos \beta} , \\ R_{b3} &= \frac{m_t^2 \sin \alpha \cot \beta}{\sin \beta} + \frac{m_b^2 \cos \alpha \tan \beta}{\cos \beta} , \\ R_{b4} &= \frac{m_t^2 \cos \alpha \cot \beta}{\sin \beta} - \frac{m_b^2 \sin \alpha \tan \beta}{\cos \beta} , \end{aligned} \quad (16)$$

where $C_{\pm\mp}^J(\theta)$ describe the process-independent part of these limits, while R_{bk} are again real and depend on the process.

It is important to remark that the relative phase of $C_{\pm\mp}^I(\theta)$ and $C_{\pm\mp}^J(\theta)$, defined by the asymptotic limits in (15) and (16), is always $\pi/2$. This is due to CP invariance in our model, and the fact that the product of the CP eigenvalues in each pair of the final neutrals is always +1 for class a, and -1 for class b.

- Class c: It contains the 3 charged boson processes (k=1,3)

$$G^+ G^- , G^+ H^- , H^+ H^- .$$

The corresponding HC amplitudes $F_{\pm\mp}^k$ at high energies may then be expressed as

$$F_{\pm\mp}^k \rightarrow R_{ck}^I C_{\pm\mp}^I(\theta) + R_{ck}^J C_{\pm\mp}^J(\theta) , \quad (17)$$

using the same angular dependent functions as in (15, 16). The corresponding couplings in (17) are again real and given by

$$\begin{aligned} R_{c1}^I &= m_t^2 + m_b^2 = R_{a1} , \quad R_{c1}^J = m_t^2 - m_b^2 \simeq R_{a1} , \\ R_{c2}^I &= m_t^2 \cot \beta - m_b^2 \tan \beta = R_{a2} , \quad R_{c2}^J = m_t^2 \cot \beta + m_b^2 \tan \beta , \\ R_{c3}^I &= m_t^2 \cot^2 \beta + m_b^2 \tan^2 \beta = R_{a3} , \quad R_{c3}^J = m_t^2 \cot^2 \beta - m_b^2 \tan^2 \beta . \end{aligned} \quad (18)$$

Since the relative phase of the two terms in (17) is always $\pi/2$, there is never any interference between them, in the differential cross sections.

To recapitulate on the $gg \rightarrow HH'$ processes in MSSM, we note that the high energy limits of the dominant HC amplitudes $F_{\pm\mp}$ in (15-18), are determined by the quark boxes in Fig.1. As the energy decreases to intermediate values, the relative magnitudes of the HC amplitudes for the various processes are changed, due to squark contributions that start becoming important. In addition to it, the HV amplitudes $F_{\pm\pm}$ also become important, at intermediate energies.

3.2 Analytical results for $gg \rightarrow VH$ in MSSM

The helicity structure (shown in (12)) is now richer than for the $gg \rightarrow HH'$ case. But the HCns rule greatly simplifies its asymptotic structure in MSSM, predicting that $F_{\pm\mp 0}$ dominates, while all other amplitudes must be vanishing.

Again, it is possible to understand analytically many of the high energy properties of these amplitudes, by looking at the diagrams of Fig.2 [23]. Using the names for the diagrams indicated in this figure, we find that:

- The HC amplitudes $F_{\pm\mp 0}$, which satisfy $\mu + \mu' - \tau = 0$, are the only ones that do not vanish asymptotically, and tend instead to "constants". This comes from combining the contributions of the various diagrams in Fig.2. The high energy values of these amplitudes may most easily be obtained by using the equivalence theorem [22], which respectively relates $F_{\pm\mp 0}$ for

$$gg \rightarrow Z_{\tau=0}G^0, Z_{\tau=0}A^0, Z_{\tau=0}H^0, Z_{\tau=0}h^0, W_{\tau=0}^+G^-, W_{\tau=0}^+H^-,$$

to the $F_{\pm\mp}$ amplitudes for

$$gg \rightarrow G^0G^0, G^0A^0, G^0H^0, G^0h^0, G^+G^-, G^+H^-,$$

determined in (15-18).

A "constant" asymptotic behaviour for $F_{\pm\mp 0}$ in $gg \rightarrow VH$ turns out to be true in SM also; but in this later case, some of the HV amplitudes may also tend asymptotically to comparable "constants".

- For amplitudes with $(\mu = \mu', \tau = 0)$, we always have $|\mu + \mu' - \tau| = 2$. In this case, non-vanishing asymptotic contributions may only come from the diagrams F , H and A . Their sum is always strongly suppressed, though, forcing these amplitudes to vanish quickly at high energies.
- For amplitudes with $\mu = \mu' = -\tau$, which always satisfy $|\mu + \mu' - \tau| = 3$, non-vanishing asymptotic contributions only come from the F and H boxes. These boxes are very small in this case, and strongly canceling each other. Therefore,

$F_{\pm\pm\mp}$ are very small and quickly vanishing at high energies. In fact, these amplitudes are vanishing at high energies faster, than those of the previous item.

- We next turn to amplitudes satisfying $|\mu + \mu' - \tau| = 1$, for processes involving neutral final particles. These HV amplitudes receive their asymptotic contributions from the F and H diagrams of Fig.2; with their sum often behaving like $\sim m/\sqrt{s}$, and thus being strongly suppressed.

Occasionally though, this suppression is reduced by a $\ln^2(s)$ factor, which makes their vanishing very slow. Below we list only these slowly vanishing amplitudes, for the relevant MSSM processes. Their high energy structure is determined by⁷

$$F_{\mu\mu'\tau} \sim \sum_{q=t,b} \frac{\alpha_s \alpha (2I_3^q) m_q^2 \sqrt{s} \sin \theta}{8\sqrt{2} s_W^2 c_W m_W} \tilde{F}_{\mu\mu'\tau} \quad , \quad (19)$$

with

$$\begin{aligned} \tilde{F}_{+++} &\simeq \left(\frac{1}{t} - \frac{1}{u} \right) \ln^2 \left(\frac{-s}{m_q^2} \right) + \left(\frac{1}{t} + \frac{1}{u} \right) \left[\ln^2 \left(\frac{-t}{m_q^2} \right) - \ln^2 \left(\frac{-u}{m_q^2} \right) \right] \quad , \\ \tilde{F}_{+--} &\simeq -\frac{1}{t} \left[\ln^2 \left(\frac{-s}{m_q^2} \right) - \ln^2 \left(\frac{-t}{m_q^2} \right) - \ln^2 \left(\frac{-u}{m_q^2} \right) \right] \quad , \\ \tilde{F}_{+--} &\simeq \frac{1}{u} \left[\ln^2 \left(\frac{-s}{m_q^2} \right) - \ln^2 \left(\frac{-t}{m_q^2} \right) - \ln^2 \left(\frac{-u}{m_q^2} \right) \right] \quad . \end{aligned} \quad (20)$$

Corresponding expressions for the amplitudes related to them by Bose statistics and CP-invariance, may be obtained from (11) for neutral final bosons. Note that the non-vanishing contributions in (19, 20) solely arise from the t and b quarks; and that they indeed have an $(m/\sqrt{s}) \ln^2 s$ -behaviour⁸. Depending on the neutral final state, the corresponding slowly vanishing amplitudes for the various MSSM processes are:

Process $gg \rightarrow ZH^0$: The slowly vanishing HV amplitudes are given by (19, 20), provided we include the extra factors $(\sin \alpha / \sin \beta)$ in the top contribution, and $(\cos \alpha / \cos \beta)$ in the bottom contribution.

Process $gg \rightarrow Zh^0$: The slowly vanishing HV amplitudes are given by (19, 20), provided we include the extra factors $(\cos \alpha / \sin \beta)$ in the top contribution, and $-(\sin \alpha / \cos \beta)$ in the bottom one.

Process $gg \rightarrow ZA^0$: The slowly vanishing HV amplitudes may again be obtained from (19, 20), provided we include the extra factors $-i \cot \beta$ in the top contribution, and $-i \tan \beta$ in the bottom contribution, and a sign-change is made to F_{+--} .

⁷As already stated above, a color factor δ_{ab} is always removed from the amplitudes. Moreover I_3^q in (19) describe the third isospin component of the t and b quarks.

⁸In fact (19, 20) describe these slowly vanishing amplitudes for $gg \rightarrow ZH$ in SM, which, as observed in Section 4, "accidentally" also obeys HCns.

Process $gg \rightarrow ZG^0$: The slowly vanishing HV amplitudes are again given by (19, 20), provided an extra factor $-i$ is included for the top, and $+i$ for the bottom contributions, and an additional sign-change is made to F_{+--} .

- Finally we consider the amplitudes satisfying $|\mu + \mu' - \tau| = 1$, for the charged final state processes $gg \rightarrow W^+ \{H^-, G^-\}$. Their dominant contribution again come from the F , H boxes. In this case the constraints from Bose statistics and CP invariance are different though; see (11). Now, F_{+++} and F_{---} receive no logarithmic enhancement and vanish quickly at high energies. Thus, the only slowly vanishing HV amplitudes, behaving like $\sim (m/\sqrt{s}) \ln^2 s$, are

$$\begin{aligned}
F_{+--} &\simeq \frac{\alpha_s \alpha m_t^2 \sqrt{s} \sin \theta}{4\sqrt{2} s_W^2 m_W} \left[\ln^2 \left(\frac{-s}{m_t^2} \right) - \ln^2 \left(\frac{-t}{m_t^2} \right) - \ln^2 \left(\frac{-u}{m_t^2} \right) \right] \frac{\{\cot \beta, 1\}}{t}, \\
F_{-++} &\simeq -\frac{\alpha_s \alpha m_t^2 \sqrt{s} \sin \theta}{4\sqrt{2} s_W^2 m_W} \left[\ln^2 \left(\frac{-s}{m_t^2} \right) - \ln^2 \left(\frac{-t}{m_t^2} \right) - \ln^2 \left(\frac{-u}{m_t^2} \right) \right] \frac{\{\cot \beta, 1\}}{u}, \\
F_{+--} &\simeq -\frac{\alpha_s \alpha m_b^2 \sqrt{s} \sin \theta}{4\sqrt{2} s_W^2 m_W} \left[\ln^2 \left(\frac{-s}{m_b^2} \right) - \ln^2 \left(\frac{-t}{m_b^2} \right) - \ln^2 \left(\frac{-u}{m_b^2} \right) \right] \frac{\{\tan \beta, -1\}}{u}, \\
F_{-+-} &\simeq \frac{\alpha_s \alpha m_b^2 \sqrt{s} \sin \theta}{4\sqrt{2} s_W^2 m_W} \left[\ln^2 \left(\frac{-s}{m_b^2} \right) - \ln^2 \left(\frac{-t}{m_b^2} \right) - \ln^2 \left(\frac{-u}{m_b^2} \right) \right] \frac{\{\tan \beta, -1\}}{t}, \quad (21)
\end{aligned}$$

for H^- and G^- production respectively. Note that the magnitudes of the first two amplitudes in (21) are determined by the top mass, while those of the later two are determined by the bottom.

As the energy decreases, squark contributions will also start affecting the HC amplitudes $F_{\pm\mp 0}$. In addition to it, other amplitudes will also start contributing to these processes; most notably the purely transverse amplitudes discussed in (19, 20, 21).

3.3 Asymptotic R_i relations in MSSM

We next turn to the so called $\tilde{\sigma}$ -quantities

$$\begin{aligned}
\tilde{\sigma}(gg \rightarrow HH') &\equiv \frac{512\pi s^{3/2}}{\alpha^2 \alpha_s^2} \frac{d\sigma(gg \rightarrow HH')}{p \, d\cos\theta}, \\
\tilde{\sigma}(gg \rightarrow VH) &\equiv \frac{512\pi s^{3/2}}{\alpha^2 \alpha_s^2} \frac{d\sigma(gg \rightarrow VH)}{p \, d\cos\theta}, \quad (22)
\end{aligned}$$

which should be measurable at a hadronic collider; see (10, 13). In MSSM, where HCNs is satisfied, the dimensionless $\tilde{\sigma}$ quantities behave asymptotically like angle-dependent "constants", solely determined by the HC amplitudes; while in SM some HV amplitudes

may also contribute at high energies. From here on, all other results in this section, are valid in MSSM only.

Using (22) and the results in (15,16), we get asymptotically

$$\begin{aligned}
R_1 \Rightarrow \tilde{\sigma}(gg \rightarrow G^0 G^0) &\simeq \tilde{\sigma}(gg \rightarrow G^0 A^0) \left(\frac{R_{a1}}{R_{a2}} \right)^2 \simeq \tilde{\sigma}(gg \rightarrow A^0 A^0) \left(\frac{R_{a1}}{R_{a3}} \right)^2 \\
&\simeq \tilde{\sigma}(gg \rightarrow H^0 H^0) \left(\frac{R_{a1}}{R_{a4}} \right)^2 \simeq \tilde{\sigma}(gg \rightarrow h^0 h^0) \left(\frac{R_{a1}}{R_{a5}} \right)^2 \simeq \tilde{\sigma}(gg \rightarrow H^0 h^0) \left(\frac{R_{a1}}{R_{a6}} \right)^2 \\
&\simeq \tilde{\sigma}(gg \rightarrow Z^0 G^0) \simeq \tilde{\sigma}(gg \rightarrow Z^0 A^0) \left(\frac{R_{a1}}{R_{a2}} \right)^2, \tag{23}
\end{aligned}$$

and

$$\begin{aligned}
R_2 \Rightarrow \tilde{\sigma}(gg \rightarrow G^0 H^0) &\simeq \tilde{\sigma}(gg \rightarrow G^0 h^0) \left(\frac{R_{b1}}{R_{b2}} \right)^2 \simeq \tilde{\sigma}(gg \rightarrow A^0 H^0) \left(\frac{R_{b1}}{R_{b3}} \right)^2 \\
&\simeq \tilde{\sigma}(gg \rightarrow A^0 h^0) \left(\frac{R_{b1}}{R_{b4}} \right)^2 \\
&\simeq \tilde{\sigma}(gg \rightarrow ZH^0) \simeq \tilde{\sigma}(gg \rightarrow Zh^0) \left(\frac{R_{b1}}{R_{b2}} \right)^2. \tag{24}
\end{aligned}$$

Note that the last lines in (23, 24) receive at non-asymptotic energies also contributions from the slowly vanishing amplitudes involving transverse final vector bosons; see the discussion around (19, 20).

We can also relate the cross sections of the charged sector, to those of the neutral sector; classes a,b,c above. Thus, combining (15, 16, 17-18, 22), we obtain

$$R_3 \Rightarrow \tilde{\sigma}(gg \rightarrow G^+ G^-) \simeq \tilde{\sigma}(gg \rightarrow G^0 G^0) + \left(\frac{R_{c1}^J}{R_{b2}} \right)^2 \tilde{\sigma}(gg \rightarrow G^0 h^0), \tag{25}$$

$$R_4 \Rightarrow \tilde{\sigma}(gg \rightarrow G^+ H^-) \simeq \left(\frac{R_{c2}^I}{R_{a1}} \right)^2 \tilde{\sigma}(gg \rightarrow G^0 G^0) + \left(\frac{R_{c2}^J}{R_{b2}} \right)^2 \tilde{\sigma}(gg \rightarrow G^0 h^0), \tag{26}$$

$$R_5 \Rightarrow \tilde{\sigma}(gg \rightarrow H^+ H^-) \simeq \left(\frac{R_{c3}^I}{R_{a1}} \right)^2 \tilde{\sigma}(gg \rightarrow G^0 G^0) + \left(\frac{R_{c3}^J}{R_{b2}} \right)^2 \tilde{\sigma}(gg \rightarrow G^0 h^0), \tag{27}$$

connecting charged and neutral final states.

Eliminating the neutral channels from (25,26, 27), we obtain

$$\begin{aligned}
\tilde{\sigma}(gg \rightarrow H^+ H^-) &\simeq \frac{1}{\left(\frac{m_t^4}{\tan^2 \beta} + m_b^4 \right)} \left\{ \left(\frac{m_t^4}{\tan^4 \beta} + m_b^4 \tan^2 \beta \right) \tilde{\sigma}(gg \rightarrow G^+ G^-) \right. \\
&\left. + \left(\frac{m_t^4}{\tan^4 \beta} - m_b^4 \right) (1 - \tan^2 \beta) \tilde{\sigma}(gg \rightarrow G^+ H^-) \right\}, \tag{28}
\end{aligned}$$

which in fact is a relation among R_3 , R_4 , R_5 , that could have also been obtained directly from (17-18).

Concerning $gg \rightarrow VH$, with charged final states, we get two more relations,

$$R_6 \Rightarrow \tilde{\sigma}(gg \rightarrow G^+G^-) \simeq \tilde{\sigma}(gg \rightarrow W^+G^-) , \quad (29)$$

$$R_7 \Rightarrow \tilde{\sigma}(gg \rightarrow G^+H^-) \simeq \tilde{\sigma}(gg \rightarrow W^+H^-) , \quad (30)$$

using (22). In deriving these relations, the high energy equivalences theorem was used, and the slowly vanishing transverse amplitudes discussed in (21) were neglected. Since these relations constrain the W production processes, they should be considered in conjunction with the last two parts of (23, 24), affecting corresponding Z cross sections.

The relations R_i of (23-30) are analogous, in spirit, to those concerning the cross sections for $ug \rightarrow dW$ and $ug \rightarrow \tilde{d}_L \tilde{\chi}_i^+$, derived in [12]. At asymptotic energies, they should be very accurate, depending only on the MSSM angles β and α ; see (15, 16, 18). Provided the SUSY particles are sufficiently light, or the hadronic collider sufficiently energetic, β and α could be determined from such relations.

As the energy decreases to intermediate values, deviations appear in R_i , which are due to 2 types of contributions. The first comes from the sub-dominant HV amplitudes which are slowly vanishing, like m/\sqrt{s} times logarithmic terms. The second one, comes from the squark boxes. Thus, at intermediate energies, further model dependence is introduced, whose investigation should offer a deeper insight to the MSSM picture. At such energies, we also expect on general grounds, that R_i become better in the central angular region, away from the forward and backward angles [23].

4 Numerical results.

As already said, the helicity amplitudes for all the gluon-gluon fusion processes in (6, 7) are calculated in terms of Passarino-Veltman (PV) functions [20], using [21] and the FORTRAN codes gghhcode and ggvhcode [13]. The resulting helicity amplitudes are expressed as functions of the c.m. energy and angle, in either the SM or the MSSM models. Input couplings and masses are always assumed to be real and at the electroweak scale, while the quark masses of the first two generations are neglected. The output files generated after running the various codes, are specified as ".dat" for the $gg \rightarrow HH'$ case; and as ".dat1, .dat2" for the $gg \rightarrow VH$ case. An accompanying Readme, fully explains the compilation of the codes.

In the figures presented here, we can only give examples of the helicity amplitudes for the various processes. Thus, for $gg \rightarrow HH'$, we just plot the two independent amplitudes F_{++}, F_{+-} ; see (6, 8, 9). Correspondingly, for $gg \rightarrow VH$, the figures contain the six independent amplitudes $F_{+++}, F_{++-}, F_{++0}, F_{+-+}, F_{+--}, F_{+-0}$, for neutral final particles;

while in the charged case, the amplitudes F_{---} , F_{--0} and F_{--+} are also included; see (7, 11, 12).

As a first example, Fig.3 shows the HC and HV amplitudes for $gg \rightarrow h^0 h^0$, in both, the MSSM benchmark $SPS1a'$ [8], and in the SM cases. Panel (a) addresses the MSSM amplitudes (F_{+-} , F_{++}), in a sufficiently high energy region elucidating the asymptotic behavior; while panel (b) is restricted to a more LHC-type energy range. Panels (c, d) give the corresponding amplitudes for $gg \rightarrow HH$ in SM.

As shown in Fig.3, above 6 TeV, the HC amplitude for this process strongly dominates in MSSM, but not in SM.

In fact, the SM process $gg \rightarrow HH$, constitutes an example where HCns is strongly violated in SM. Similar violations of HCns in SM, may also been seen for $gg \rightarrow G^0 G^0$ in Fig.4a; and for $gg \rightarrow W^+ G^-$ in Fig.5a,b. Because of these and the equivalence theorem, a clear violation of HCns for the SM processes $gg \rightarrow ZG^0$ and $gg \rightarrow G^+ G^-$ is also true. These are the only known examples where HCns is not even approximately obeyed in SM.

Contrary to them, the corresponding MSSM results in Figs.4b and 5c,d satisfy helicity conservation.

A peculiarity arises for the SM process $gg \rightarrow ZH$ presented in Fig.6, and the corresponding MSSM process $gg \rightarrow Zh^0$ shown in Fig.7. The validity of HCns in both cases seems equally good. A similar situation arises also for the SM process $gg \rightarrow G^0 H$ and the MSSM process $gg \rightarrow G^0 h^0$, related to the previous ones by the equivalence theorem. Such an "accidental" validity of helicity conservation for e.g. $gg \rightarrow G^0 H$ in SM, must be related to the absence of a squark contribution in the corresponding MSSM process $gg \rightarrow G^0 h^0$, which makes the SM and MSSM amplitudes very similar.

We next focus on the MSSM helicity amplitudes, always using the $SPS1a'$ benchmark [8]. As it can be seen from Fig.3b, the HV amplitude for $gg \rightarrow h^0 h^0$ vanishes very quickly with energy. But for $gg \rightarrow H^0 h^0$, $H^+ H^-$, $A^0 h^0$, this vanishing seems slower, apparently due to a larger squark contribution; see Figs.8, which suggest that a minimum energy of ~ 10 TeV is required, for HCns to be approximately realized.

In Figs.9 and 10 we show the amplitudes for $gg \rightarrow ZA^0$ and $gg \rightarrow W^+ H^-$. These results, together with those for $gg \rightarrow Zh^0$ (see Figs.7), indicate that the high energy vanishing of the HV amplitudes in the $gg \rightarrow VH$ cases is generally slower, than in the $gg \rightarrow HH'$ cases. Particularly for $W^+ H^-$, center of mass energies of $\gtrsim 20$ TeV are required in $SPS1a'$, for helicity conservation to approximately establish itself. Such a slow approach to the HCns regime, should be partly due to the slow vanishing of the transverse amplitudes in (21, 19, 20).

Finally, in Figs.11-14, we compare the energy- and angle-dependence of the various parts of the cross section relations R_i , defined in (23-30). These R_i -parts should always become identical at high energies; while their deviations at intermediate energies give a measure of the violations in R_i .

In the $SPS1a'$ benchmark we are using, which belongs to the so called decoupling

MSSM regime, the h^0 self-couplings, as well as its couplings to the quarks, leptons and the gauge bosons, are very close to the SM ones, implying $\alpha \simeq \beta - \pi/2$ [25]. Through (15-18), this leads to

$$\begin{aligned} R_{a4} &\simeq R_{a3} , \quad R_{a5} \simeq R_{a1} , \quad R_{a6} \simeq -R_{a2} , \\ R_{b1} &\simeq -R_{b4} \simeq -R_{c2}^J , \quad R_{b2} \simeq R_{c1}^J , \quad R_{b3} \simeq -R_{c3}^J , \end{aligned}$$

which explain many features in Figs.11-14.

Concentrating on R_1 defined in (23), we compare in Figs.11 the magnitudes of its various parts; here panels (a,b) describe the energy dependencies at ($\theta = 30^\circ, 60^\circ$), while (c) gives the angular dependence at a c.m. energy $\sqrt{s} = 8$ TeV. As seen from (a,b), five of the R_1 parts reach their common asymptotic value already at ~ 6 TeV, for the above angles. Deviations persist only for the $gg \rightarrow H^0 H^0$, $H^0 h^0$ parts, which seem to come from squark boxes⁹; and for the $gg \rightarrow ZG^0$ part (related through the equivalence theorem to $gg \rightarrow ZZ_{\text{longitudinal}}$), which is due to the slowly vanishing contributions discussed in (19,20). Energies of $\gtrsim 20$ TeV are needed for all these R_1 deviations to fall below the 10% level.

These deviations are also reflected in Fig.11c, presenting the angular distributions of the various R_1 -parts at 8 TeV.

In Figs.12, the corresponding results for R_2 defined in (24), are presented. At an energy of ~ 8 TeV and angles in the central region, R_2 is much better satisfied than R_1 .

In Figs.13, the left and right parts of (R_3, R_4, R_5) defined in (25-27) are compared; panels (a,b) gives the energy- and angle-dependence for R_3 , (c,d) correspondingly for R_4 , and (e,f) for R_5 . The agreement between the left and right parts in the central region is rather poor, at an energy of ~ 8 TeV. In fact for R_4 , even the shapes of the two parts are different at 8 TeV. As the energy increases, these relations gradually improve; the deviations reducing to the 20% level at 20 TeV, and to the permille level at 400 TeV.

Finally in Figs.14, we compare the left and right parts of R_6, R_7 defined in (29, 30); again (a,b) give the energy- and angle-dependencies for R_6 , and (c,d) the corresponding results for R_7 . At an energy scale of $\gtrsim 12$ TeV, these relations are satisfied for angles in the central region. It appears, that the squark boxes and the HV amplitudes for the WG, WH channels, are responsible for most of the deviations at $\lesssim 12$ TeV.

At least, as far as the contribution from the $gg \rightarrow VH$ processes is concerned, we could, in principle extend the validity of the relations R_1, R_2, R_6, R_7 to lower energies, by subtracting the contributions from the slowly vanishing transverse amplitudes discussed in Sections 3.2. This, will of course make these relations considerably more

⁹For $gg \rightarrow G^0 G^0, G^0 A^0, A^0 A^0$, the approach to asymptopia is faster because the squark plus anti-squark box contributions vanish identically.

complicated.

Of course, the appearance of helicity conservation, as well as the validity of the asymptotic R_i relations discussed above, will be further delayed, if the SUSY masses are higher than those at $SPS1a'$.

In any case, using the codes [13] which give the exact 1loop EW predictions for the above amplitudes, the exact values of all separate parts of the R_i relations in (23-30) may be calculated, and its validity checked, for any MSSM model at any energy.

5 Summary and outlook

The helicity conservation theorem, proved to all orders, for any 2-to-2 process at asymptotic energies and fixed angles, is a really impressive property of any supersymmetric extension of SM [4].

It not only greatly simplifies the structure of the asymptotic amplitudes, but it may also have important implications at realistic LHC energies, provided the SUSY scale is not too high. This has been realized for a considerable range of MSSM benchmarks, by studying the complete 1loop EW contributions to $ug \rightarrow dW$ [7]; as well as by constructing asymptotic cross section relations between $ug \rightarrow dW$ and $ug \rightarrow \tilde{d}_L \tilde{\chi}_j^+$, which were seen to remain approximate correct even close to the LHC range [12].

In all examples studied previously, which were all done at the 1loop EW order in MSSM, the dominant helicity conserving amplitudes were always increasing logarithmically, whilst the helicity violating ones were tending to zero.

Comparing to corresponding 1loop SM results for processes with standard external particles, it appeared that HCns is approximately correct in SM also; in the sense that the helicity conserving amplitudes were again found to increase logarithmically with energy, while the HV ones were going to much smaller "constants". In fact, in such cases, the dominance of the logarithmically increasing HC amplitudes is often so overwhelming, that it should be impossible to experimentally discriminate a "constant" asymptotic value of an HV SM amplitude, from a strictly vanishing one; see e.g. the example of $\gamma\gamma \rightarrow \gamma\gamma$, $Z\gamma$, ZZ in [6].

In the present work we looked at processes where the dominant HC amplitudes cannot be very large, so that to obtain a more stringent view of the way HCns is realized. Thus, we looked at the 1loop EW predictions for processes where there are no gauge (or gaugino) contributions within 1loop; and thus, no large logarithmic enhancements. In this spirit, we have studied the 13 processes $gg \rightarrow HH'$ and the 6 processes $gg \rightarrow VH$, within any CP conserving MSSM framework; see (6, 7).

Correspondingly in SM, we have calculated the 1loop EW predictions for the 4 $gg \rightarrow HH'$ processes, and the 3 $gg \rightarrow VH$ processes; see again (6, 7). And for the first time, we indeed saw examples where helicity conservation is strongly violated in SM.

In MSSM, of course, HCns is always obeyed. These detail examples confirm that helicity conservation indeed is a genuine SUSY property; in accordance with the general, rather formal, all order proof in [4].

The most striking example of difference between SM and MSSM is in the process $gg \rightarrow h^0 h^0$, as one can see in Fig.3. In SM, the HV amplitude for this process tends to a constant value, which is about half the value of the helicity conserving one. Contrary to it, in MSSM an opposite contribution from the squark loop arises, which exactly cancels the HV amplitude at energies much larger than the squark masses. The unpolarized cross sections in the two cases should then differ by about 20% at sufficiently high energies, which could be observable, particularly if squark candidates are also observed in the TeV range.

FORTTRAN codes calculating the helicity amplitudes of all processes in (3, 6, 7), as functions of the center of mass energy and angle, are released in [13]. The input parameters in these codes are always at the electroweak scale, while the quark masses of the first two generations are neglected.

In this work, we have also derived the $R_1 - R_7$ asymptotic relations among various cross sections, within the MSSM framework. Strictly speaking these relations should be exact (to the 1loop EW order of course) at asymptotic energies and fixed angles. The only MSSM parameters they depend on, are the α and β MSSM angles. Testing such relations (at sufficiently high energies), would constitute a genuine check of the MSSM structure.

As the energy decreases though, deviations in the $R_1 - R_7$ relations appear, like those shown in Figs.11-14 for $SPS1a'$ [8]. We have studied in detail these relations in $SPS1a'$; and as a general statement we could say that at an energy of $\gtrsim 8$ TeV, they are satisfied to an accuracy of $\sim 50\%$ or better. Of course the accuracy of these relations would become better or worse, depending on whether the SUSY scale is lower or higher than in this benchmark.

The energies needed for R_i to acquire a certain accuracy, are generally larger than those required for the relation connecting the $ug \rightarrow dW$ and $ug \rightarrow d_L \tilde{\chi}_i^+$ cross sections [12]. This is probably due to the presence of important Born contributions to these later processes, which makes them less sensitive to higher scale-effects, than the purely 1loop processes entering the R_i 's.

We also note that the departures from the asymptotic predictions $R_1 - R_7$ arise from global SUSY-scale effects. Measuring such effects could define a strategy of SUSY analysis, starting from the high energy range where the basic SUSY properties can be established, and then going down in energy, progressively becoming more sensitive to specific SUSY masses. Such a strategy is to be opposed to the usual one starting from the low energy with more than 100 free parameters in MSSM, and then going up in energy. If the SUSY scale is not too high, such a strategy may be feasible.

In the near future we hope to look at the 1loop EW predictions for the gluon-gluon fusion producing two vector bosons, or two charginos or neutralinos [26]. We expect that the combination of these processes, with those studied here, will supply many more asymptotic relations among various, in principle measurable, cross sections .

In conclusion, we dare to say that the SUSY best motivated candidacy for describing the physics beyond SM, is not only due to its smooth ultraviolet properties, its inclusion of dark matter candidates, and its invitation to unification. Its exact helicity conservation property for any 2-to-2 process, which so strongly simplifies its asymptotic amplitudes, also deserves to be added to this list.

Acknowledgements

G.J.G. gratefully acknowledges the support by the European Union contracts MRTN-CT-2004-503369 and HEPTOOLS, MRTN-CT-2006-035505.

References

- [1] M. Beccaria, F.M. Renard and C. Verzegnassi, hep-ph/0203254; "Logarithmic Fingerprints of Virtual Supersymmetry", Linear Collider note LC-TH-2002-005, GDR Supersymmetrie note GDR-S-081. M. Beccaria, M. Melles, F. M. Renard, S. Trimarchi, C. Verzegnassi, Int. J. Mod. Phys. **A18**:5069 (2003), hep-ph/0304110.
- [2] for a review and a rather complete set of references see e.g. A. Denner and S. Pozzorini, Eur. Phys. J. **C18**:461 (2001); A. Denner, B. Jantzen and S. Pozzorini, Nucl. Phys. **B761**:1 (2007), hep-ph/0608326.
- [3] G.J. Gounaris, J. Layssac and F.M. Renard, Phys. Rev. **D67**:013012 (2003), hep-ph/0211327; a longer version of this work has also appeared hep-ph/0207273.
- [4] G.J. Gounaris and F.M. Renard, Phys. Rev. Lett. **94**:131601 (2005), hep-ph/0501046; Addendum in Phys. Rev. **D73**:097301 (2006), hep-ph/0604041.
- [5] G.J. Gounaris, Acta Phys. Polon. **B37**:1111 (2006) , hep-ph/0510061.
- [6] G.J. Gounaris, P.I. Porfyriadis and F.M. Renard, Eur. Phys. J. **C9**:673 (1999), arXiv:hep-ph/9902230. G.J. Gounaris, J.Layssac, P.I. Porfyriadis and F.M. Renard, Eur. Phys. J. **C10**:499 (1999), arXiv:hep-ph/9904450. G.J. Gounaris, J.Layssac, P.I. Porfyriadis and F.M. Renard, Eur. Phys. J. **C13**:79 (2000), arXiv:hep-ph/9909243. G.J. Gounaris, P.I. Porfyriadis and F.M. Renard, Eur. Phys. J. **C19**:57 (2001), arXiv:hep-ph/00100006.
- [7] G.J. Gounaris, J. Layssac and F.M. Renard, Phys. Rev. **D77**:013003 (2008), arXiv:0709.1789 [hep-ph].

- [8] J.A. Aguilar-Saavedra et al., SPA convention, Eur. Phys. J. **C46**:43 (2005), hep-ph/0511344; B.C. Allanach et al. Eur. Phys. J. **C25**:113 (2002), hep-ph/0202233.
- [9] O. Buchmueller et al., arXiv:0707.3447 [hep-ph].
- [10] H. Baer, V. Barger, G. Shaughnessy, H. Summy and L-T Wang, hep-ph/0703289
- [11] D. Feldman, Z. Liu and P. Nath, Phys. Rev. Lett. **99**:251802 (2007), arXiv:0707.1873 [hep-ph]; D. Feldman, Z. Liu and P. Nath, arXiv:0802.4085.
- [12] G.J. Gounaris, J. Layssac and F.M. Renard, Phys. Rev. **D77**:093007 (2008), arXiv:0803.0813 [hep-ph].
- [13] The FORTRAN codes together with a Readme file explaining its use, are contained in gghcode.tar.gz and ggVhcode.tar.gz, which can be downloaded from <http://users.auth.gr/gounaris/FORTRANcodes>. All input parameters in the code are at the electroweak scale.
- [14] T. Plehn, M. Spira, P.M. Zerwas, Nucl. Phys. **B479**:46 (1996), Erratum- Nucl. Phys. **B531**:655 (1998), arXiv:hep-ph/9603205; A. Krause, T. Plehn, H. Spira, P.M. Zerwas, Nucl. Phys. **B519**:85 (1998), arXiv:hep-ph/9707430.
- [15] O. Brein, W. Hollik, Eur. Phys. J. **C13**:175 (2000), arXiv:hep-ph/9908529; O. Brein, W. Hollik, S. Kanemura, Phys. Rev. **D63**:095001 (2001) arXiv:hep-ph/0008308.
- [16] Y. Jiang, L. Han, W-G Ma, Z-H Yu, M. Han, J. Phys. **G23**,385 (1997), err. J. Phys. **G23**,1151 (1997), arXiv:hep-ph/9703275; Y. Jiang, W-g Ma, L. Han, M. Han, Z-hui Yu, J. Phys. **G24**,83 (1998), arXiv:hep-ph/9708421.
- [17] M. Melles, Phys. Rep. **375**:219 (2003).
- [18] B.A. Kniehl Phys. Rev. **D42**:2253 (1990); A.A. Barrientos Bendezu, B.A. Kniehl, Phys. Rev. **D59**:015009 (1999), arXiv:hep-ph/9807480 ; A.A. Barrientos Bendezu, B.A. Kniehl, Nucl. Phys. **B568**:305 (2000), arXiv:hep-ph/9908385; A.A. Barrientos Bendezu, B.A. Kniehl, Phys. Rev. **D61**:097701 (2000), arXiv:hep-ph/9909502; A.A. Barrientos Bendezu, B.A. Kniehl Phys. Rev. **D63**:015009 (2001), arXiv:hep-ph/0007336; A.A. Barrientos Bendezu, B.A. Kniehl, Phys. Rev. **D64**:035006 (2001), arXiv:hep-ph/0103018.
- [19] S. Dawson, S. Dittmaier, M. Spira, Phys. Rev. **D58**:115012 (1998), arXiv:hep-ph/9805244; V. Ahrens, T. Becher, M. Neubert and L.L. Yang, arXiv:0808.3008.
- [20] G. Passarino and M. Veltman Nucl. Phys. **B160**:151 (1979).
- [21] T. Hahn, LoopTools, <http://www.feynarts.de/looptools/>; T. Hahn and M. Pérez-Victoria, hep-ph/9807565; G.J. van Oldenborgh and J.A.M. Vermaseren, Z. f. Phys. **C46**:425 (1990).

- [22] J.M. Cornwall, D.N. Levin, and G. Tiktopoulos, Phys. Rev. **D10**:1145 (1974); M.S. Chanowitz, and M.K. Gaillard, Nucl. Phys. **B261**:379 (1985); G.J. Gounaris, R. Kögerler and H. Neufeld, Phys. Rev. **D34**:3257 (1986); H. Veltman, Phys. Rev. **D41**:2294 (1990).
- [23] M. Beccaria, G.J. Gounaris, J. Layssac and F.M. Renard, Int. J. Mod. Phys. **A23**:1839 (2008), arXiv:0711.1067 [hep-ph]; M. Roth and A. Denner, Nucl. Phys. **B479**:495 (1996).
- [24] See e.g. J. Gunion, H. Haber, G. Kane and S. Dawson, "The Higgs Hunters Guide", Addison-Wesley, Reading, 1990.
- [25] See e.g. A. Djouadi, arXiv:0810.2439.
- [26] G.J. Gounaris, J. Layssac and F.M. Renard, in preparation.

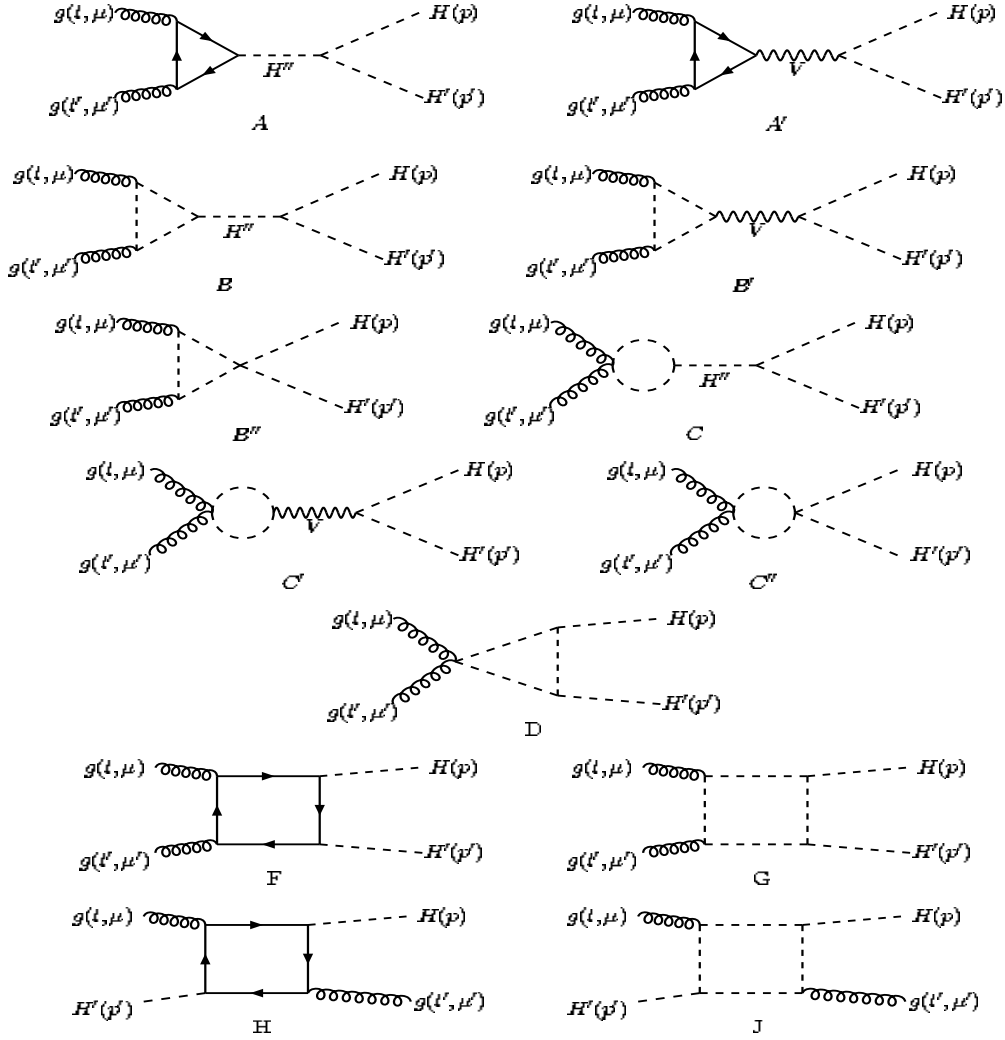


Figure 1: Independent diagrams for calculating $gg \rightarrow HH'$ in MSSM and SM; with (H, H') denoting scalar Higgs particles or Goldstone bosons. The diagrams are named as $A, A', B, B', B'', C, C', C'', D, F, G, H, J$. The s -channel scalar or vector exchanges in some of the triangular and bubble graphs are named as H'' and V . Full, broken and wavy lines describe respectively fermionic, scalar and vector particles. The incoming and outgoing momenta and helicities are indicated in parentheses.

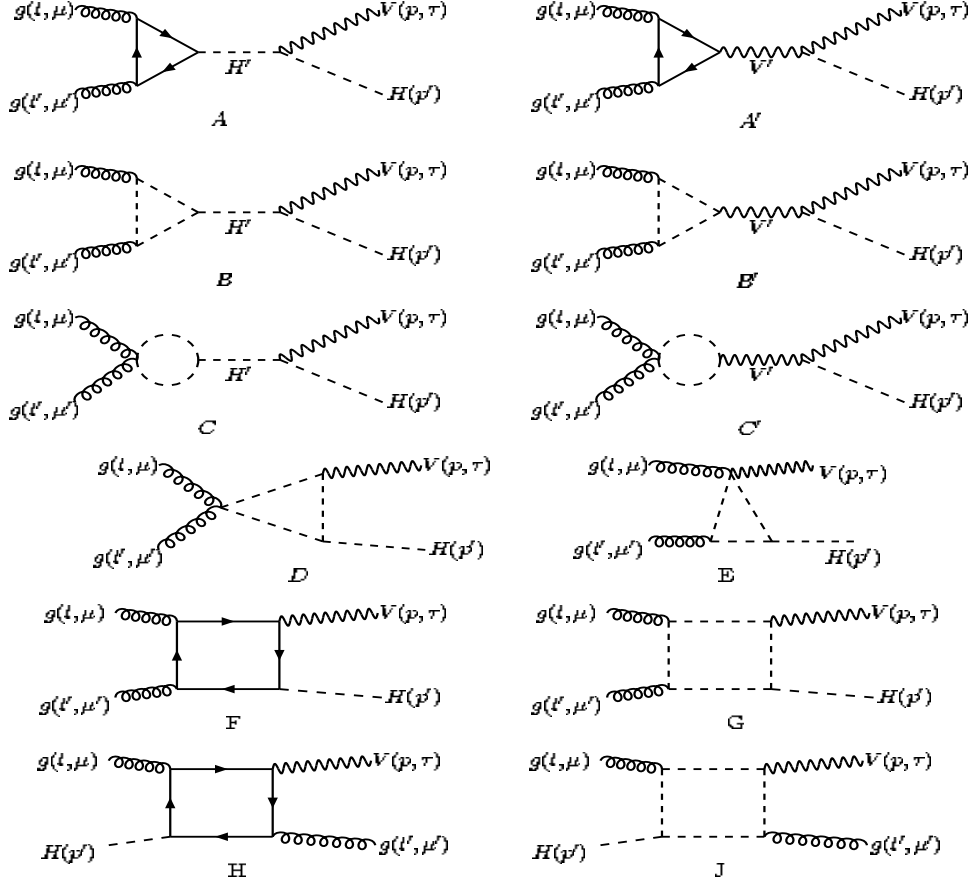


Figure 2: Independent diagrams for calculating $gg \rightarrow VH$ in MSSM and SM, with V denoting a vector particle, and H describing a scalar Higgs-type particle or Goldstone boson. The diagrams are named as $A, A', B, B', C, C', D, E, F, G, H, J$. The s -channel scalar or vector exchanges in some of the triangular and bubble graphs are named as H' and V' . Full, broken and wavy lines describe respectively fermionic, scalar and vector particles. The incoming and outgoing momenta and helicities are indicated in parentheses.

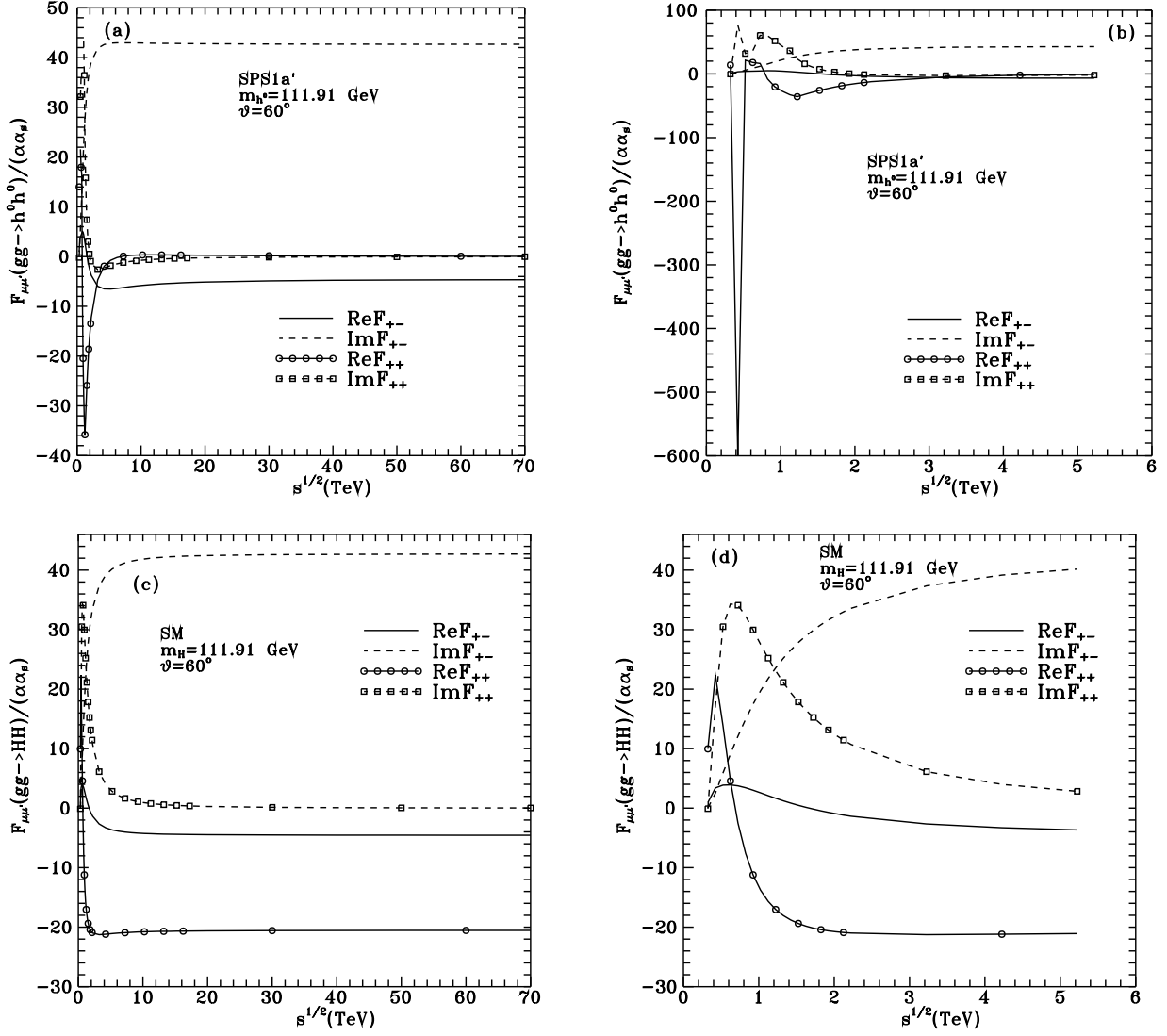


Figure 3: Amplitudes for $gg \rightarrow h^0 h^0$ in *SPS1a'* (a,b) [8], and for $gg \rightarrow HH$ in SM (c,d).

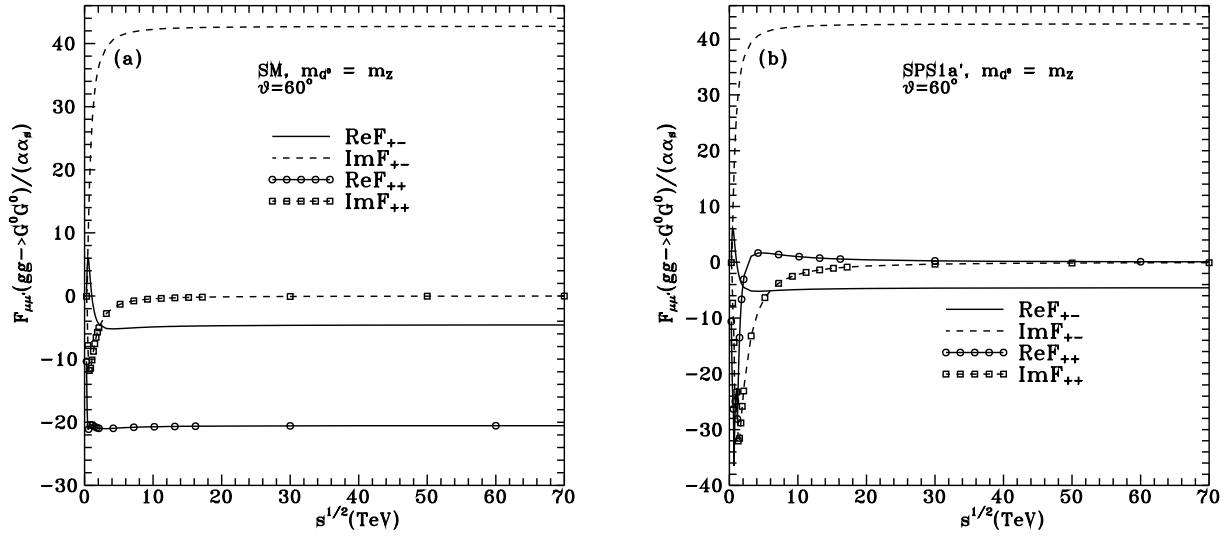


Figure 4: Amplitudes for $gg \rightarrow G^0 G^0$ in SM (a) and in $SPS1a'$ (b).

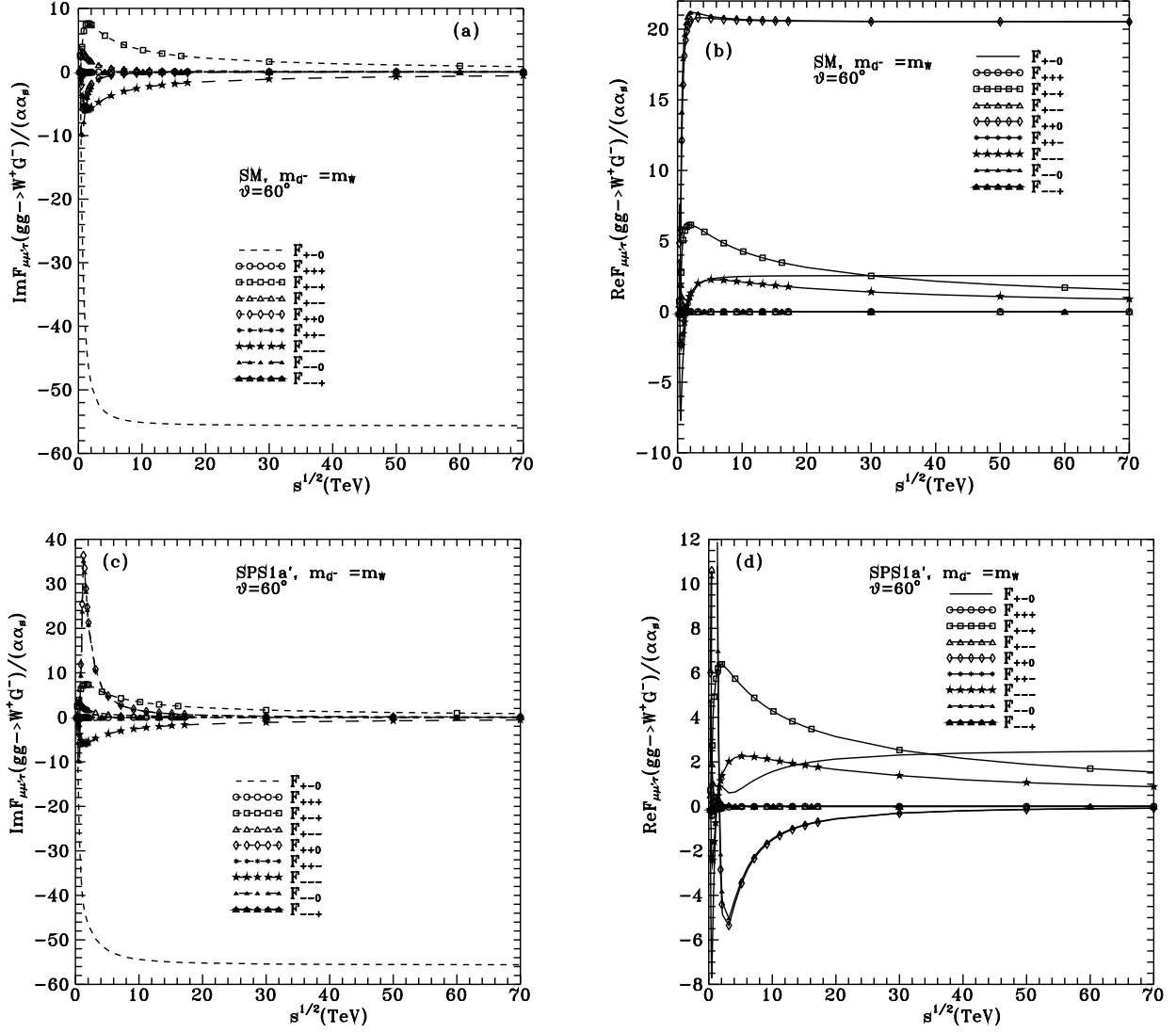


Figure 5: Amplitudes for $gg \rightarrow W^+ G^-$ in SM (a,b), and $SPS1a'$ (c,d).

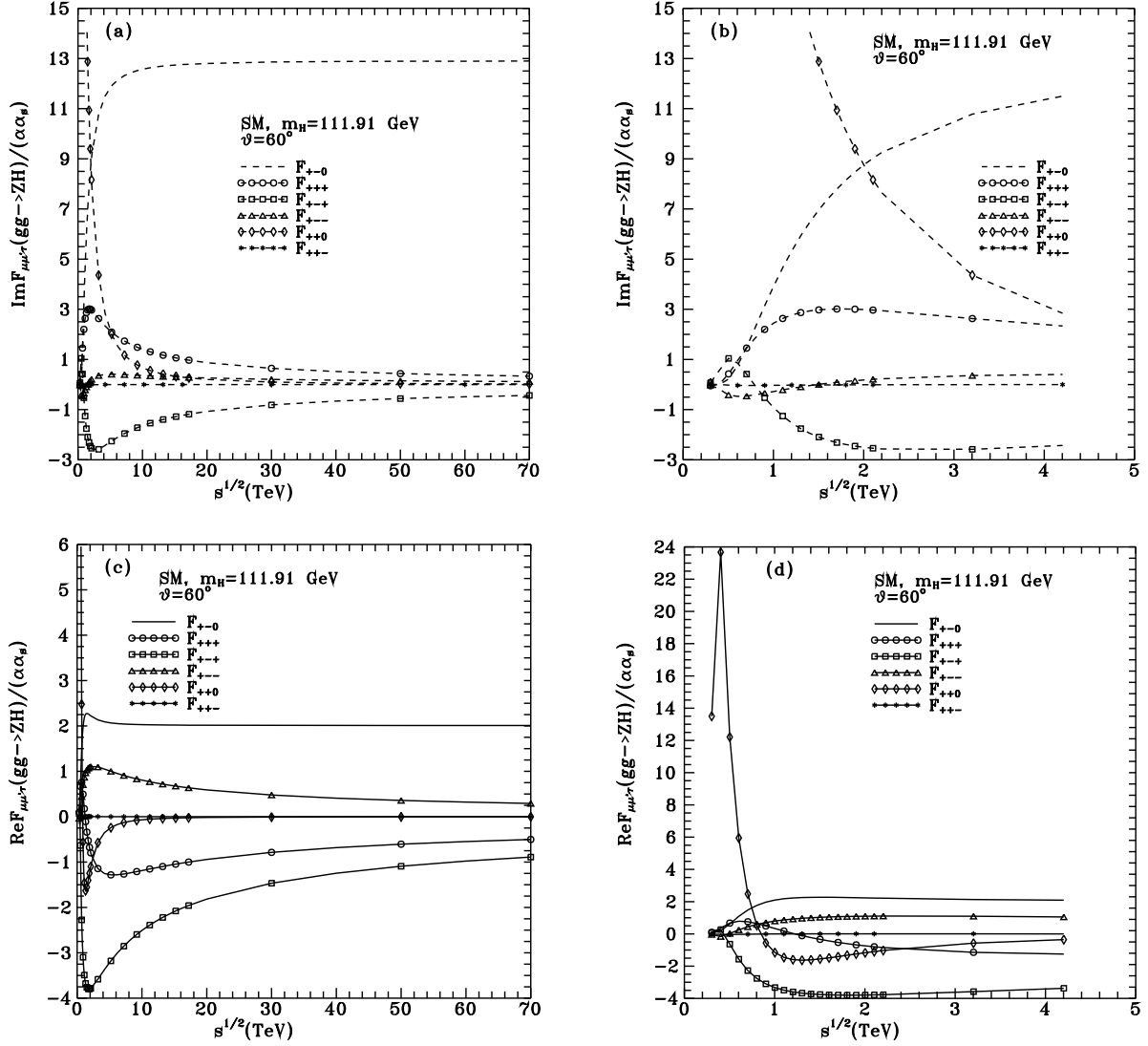


Figure 6: Amplitudes for $gg \rightarrow ZH$ in SM; (a,c) describe the high energy behaviour, while (b,d) emphasize the LHC range.

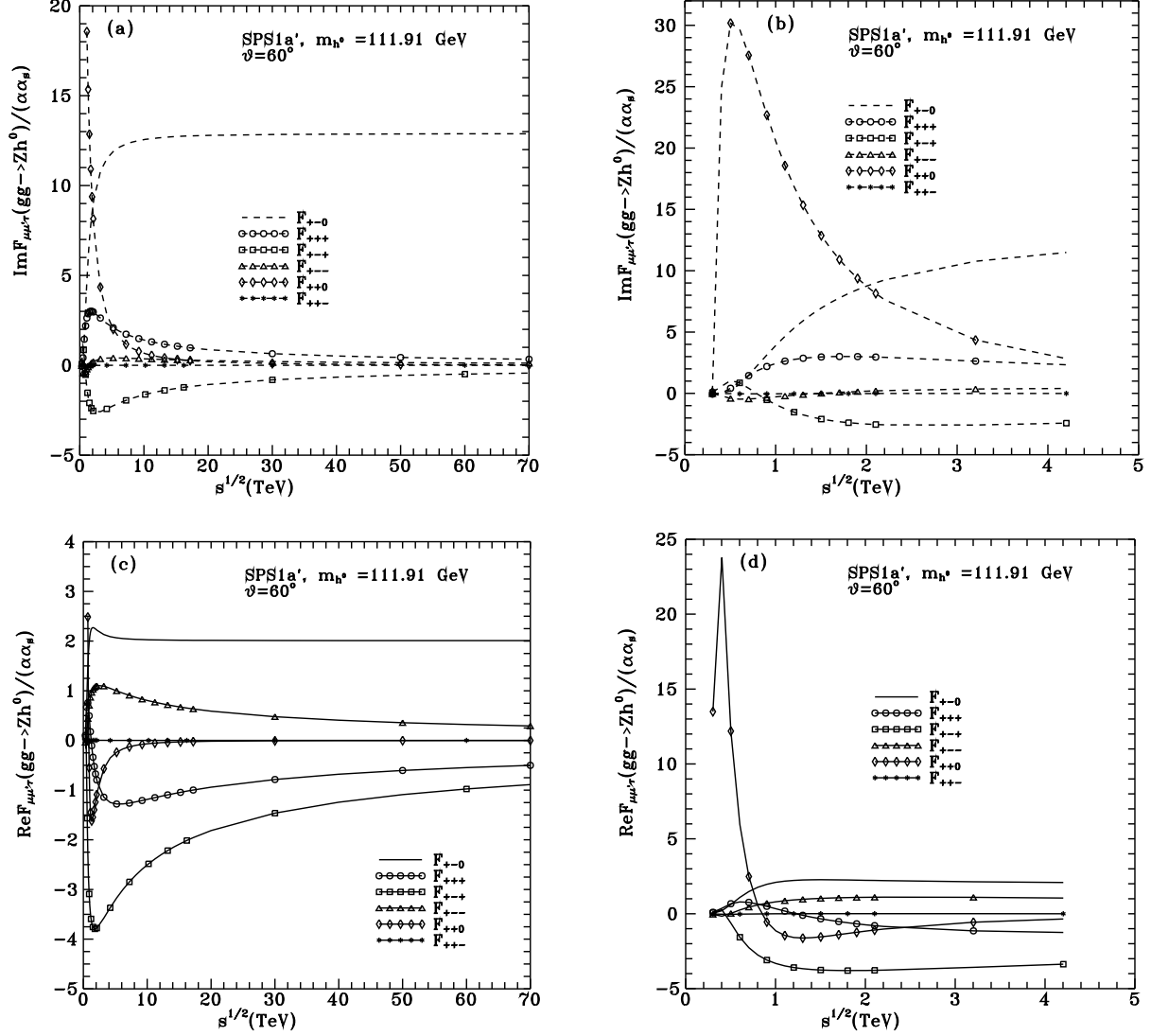


Figure 7: Amplitudes for $gg \rightarrow Zh^0$ in $SPS1a'$; (a,c) describe the high energy behaviour while (b,d) emphasize the LHC range.

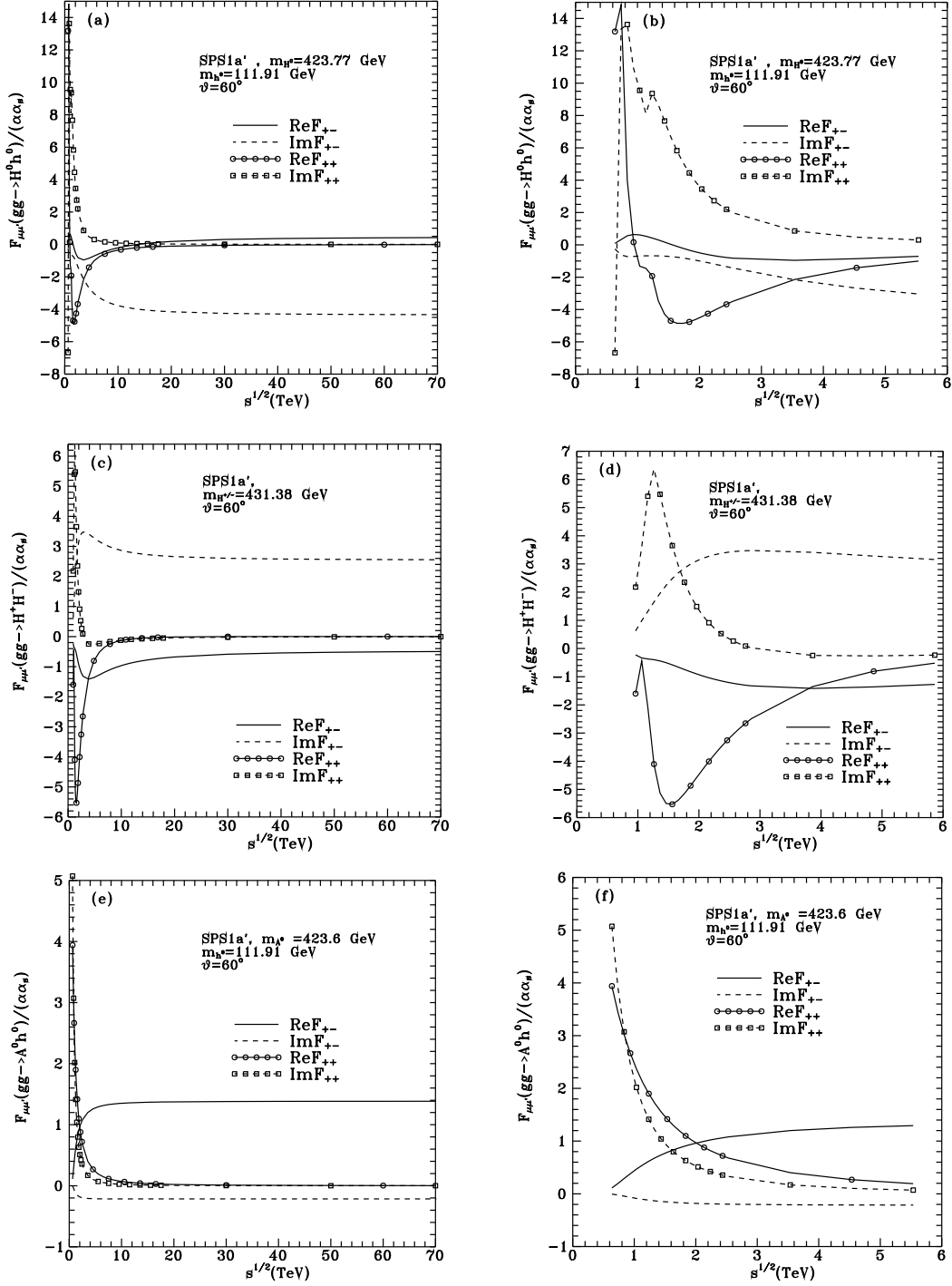


Figure 8: Amplitudes describing the high-energy and the LHC-type-energies (see previous caption) for $gg \rightarrow H^0 h^0$ (a,b), $gg \rightarrow H^+ H^-$ (c,d), and $gg \rightarrow A^0 h^0$ (e,f) in SPS1a'.

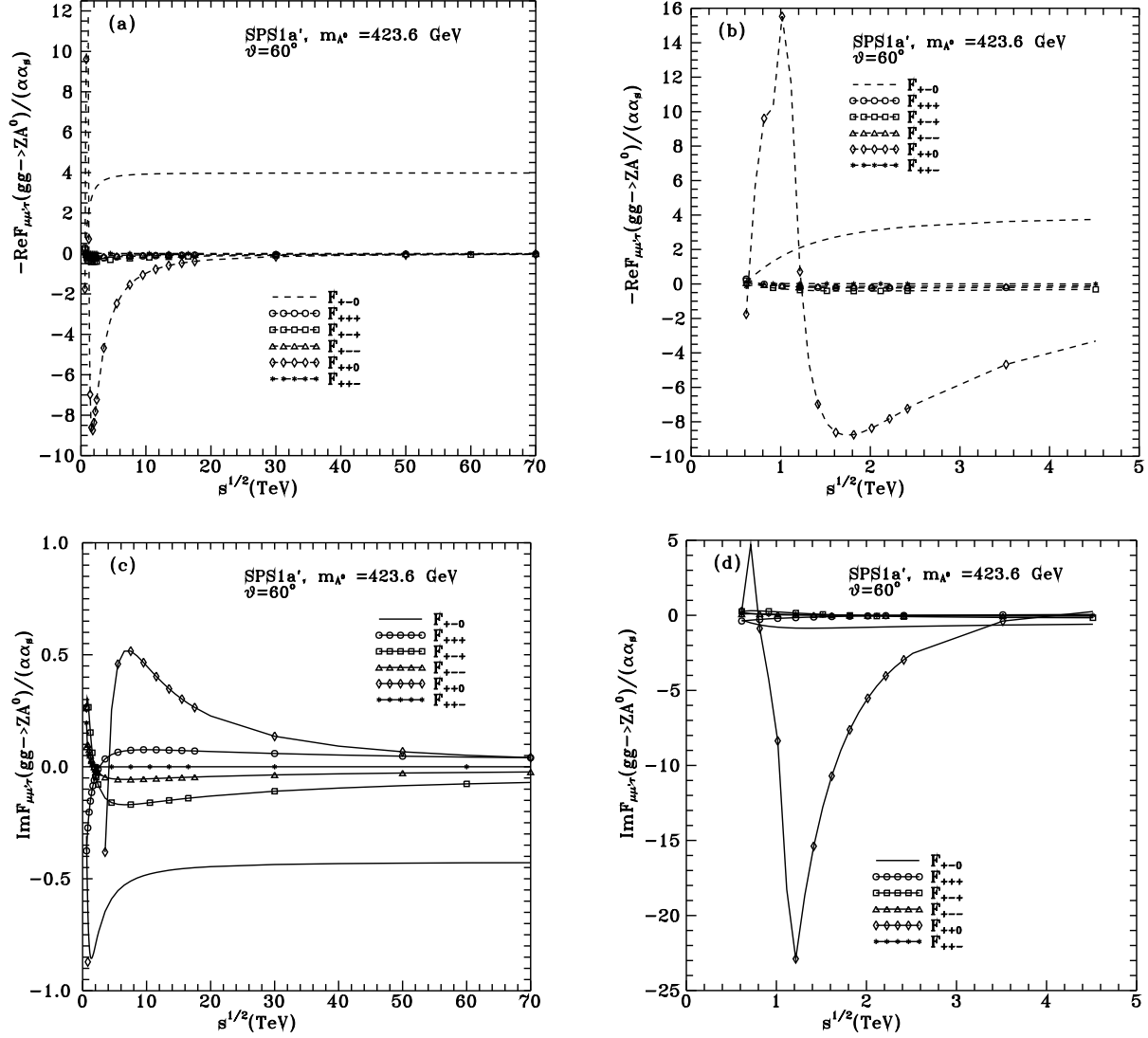


Figure 9: Amplitudes for $gg \rightarrow ZA^0$ in $SPS1a'$; (a,c) describe the high energy behaviour while (b,d) emphasize the LHC range.

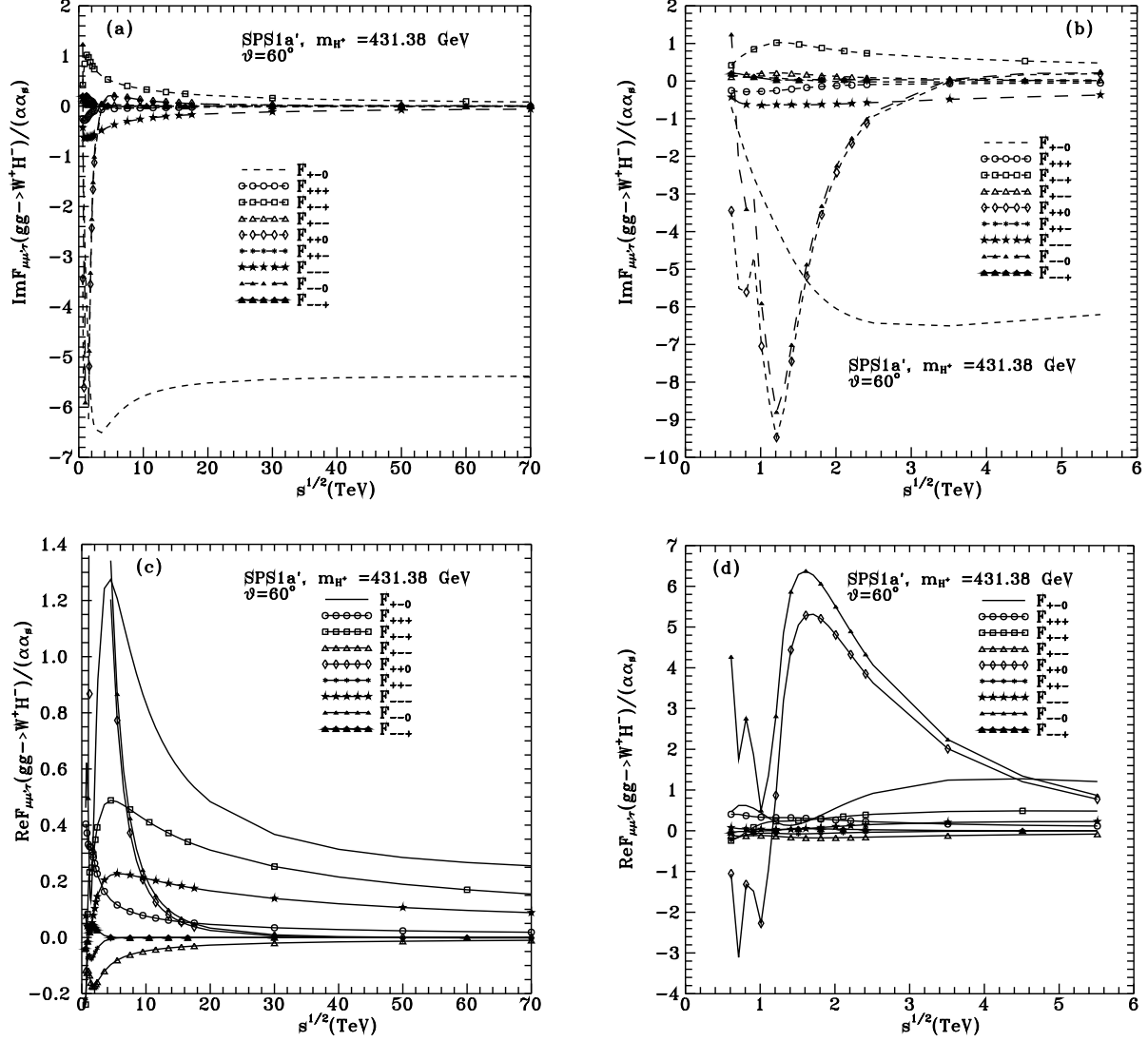


Figure 10: Amplitudes for $gg \rightarrow W^+H^-$ in $SPS1a'$; (a,c) describe the high energy behaviour while (b,d) emphasize the LHC range.

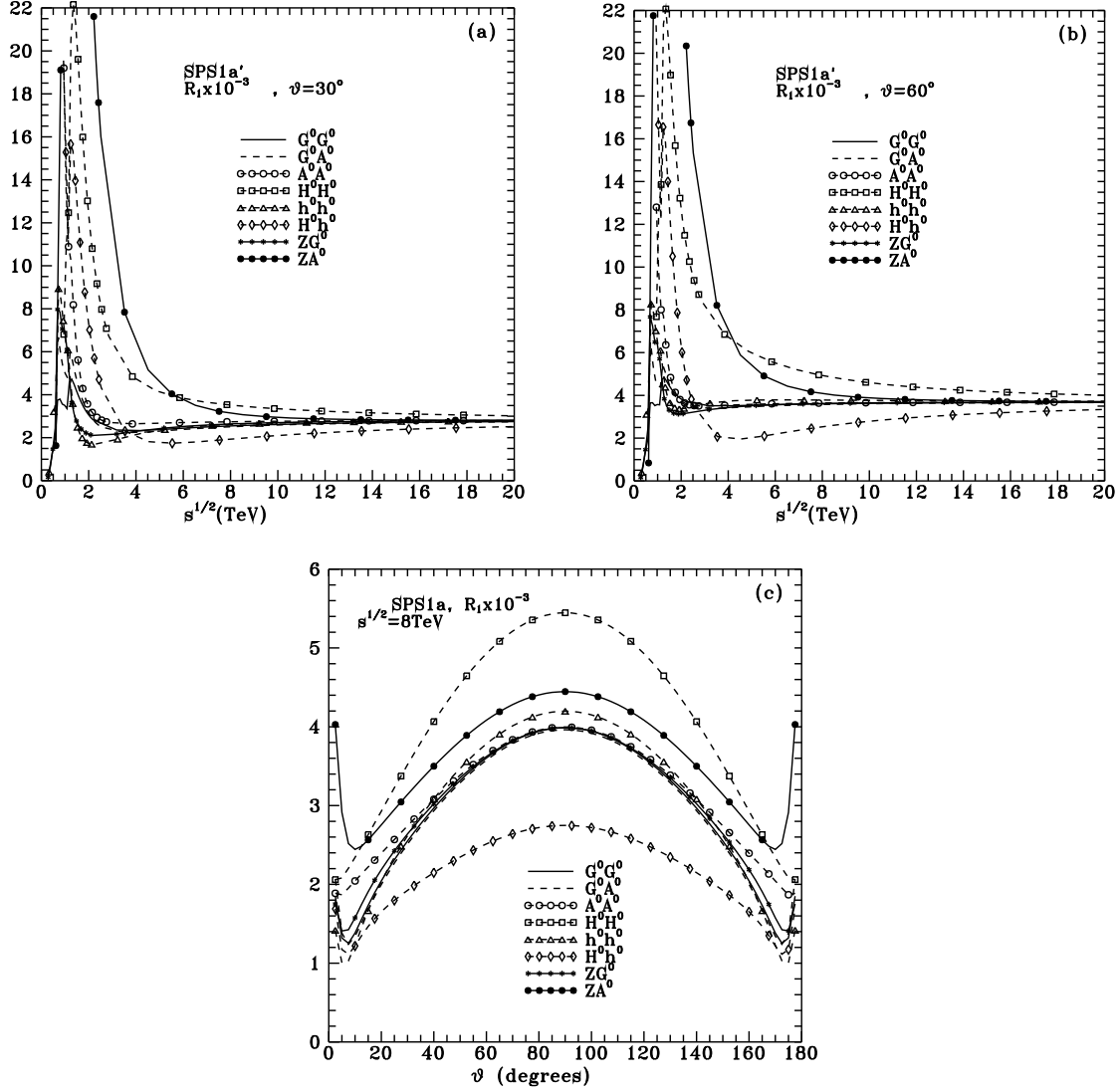


Figure 11: Magnitudes of the various parts of the asymptotic relation R_1 defined in (23); (a,b) describe the energy dependence at $\theta = 30^\circ$ and $\theta = 60^\circ$ respectively; while (c) gives the angular dependence at $\sqrt{s} = 8$ TeV.

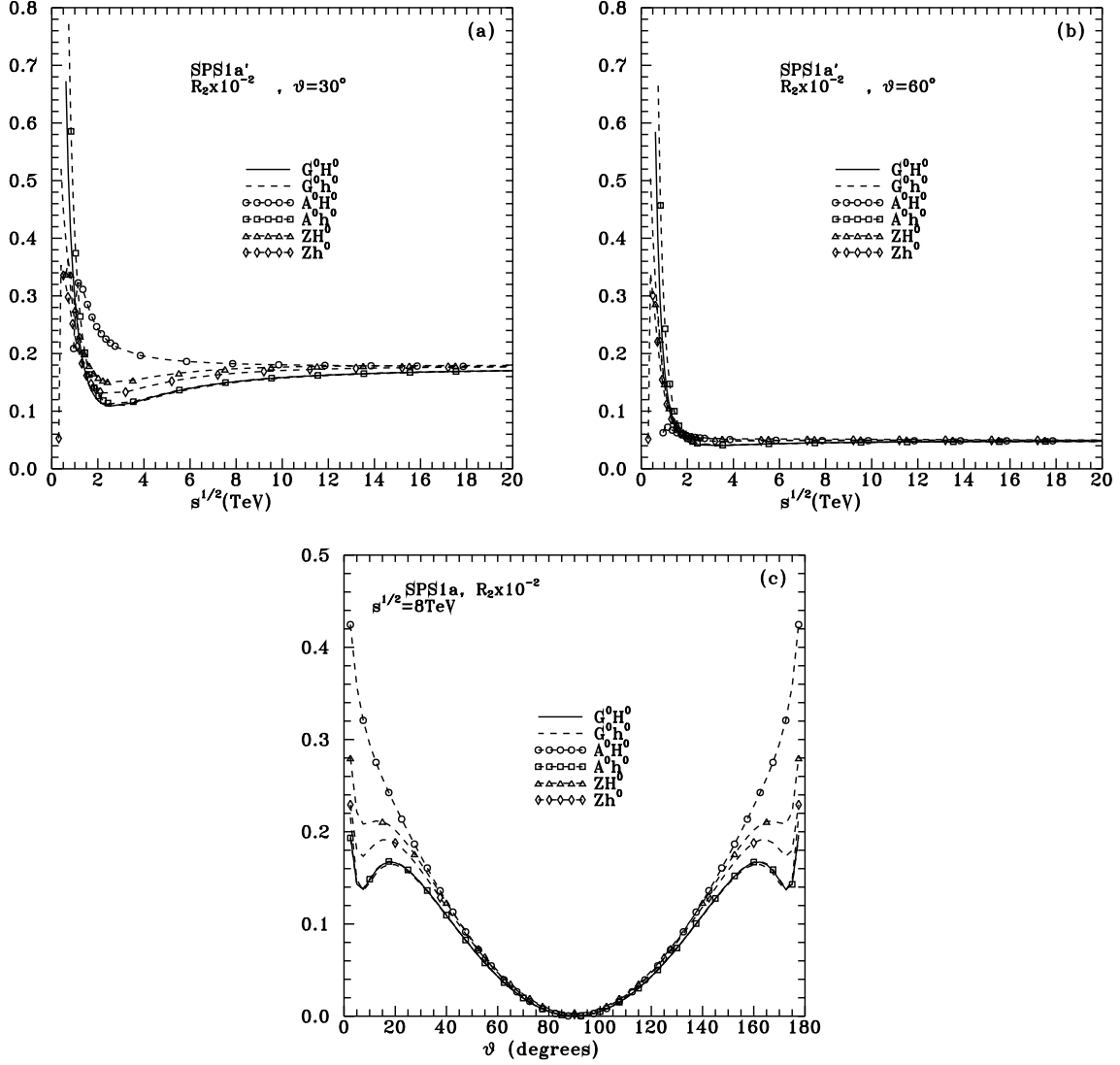


Figure 12: Magnitudes of the various parts of the asymptotic relation R_2 defined in (24); (a,b) describe the energy dependence at $\theta = 30^\circ$ and $\theta = 60^\circ$ respectively; while (c) gives the angular dependence at $\sqrt{s} = 8$ TeV.

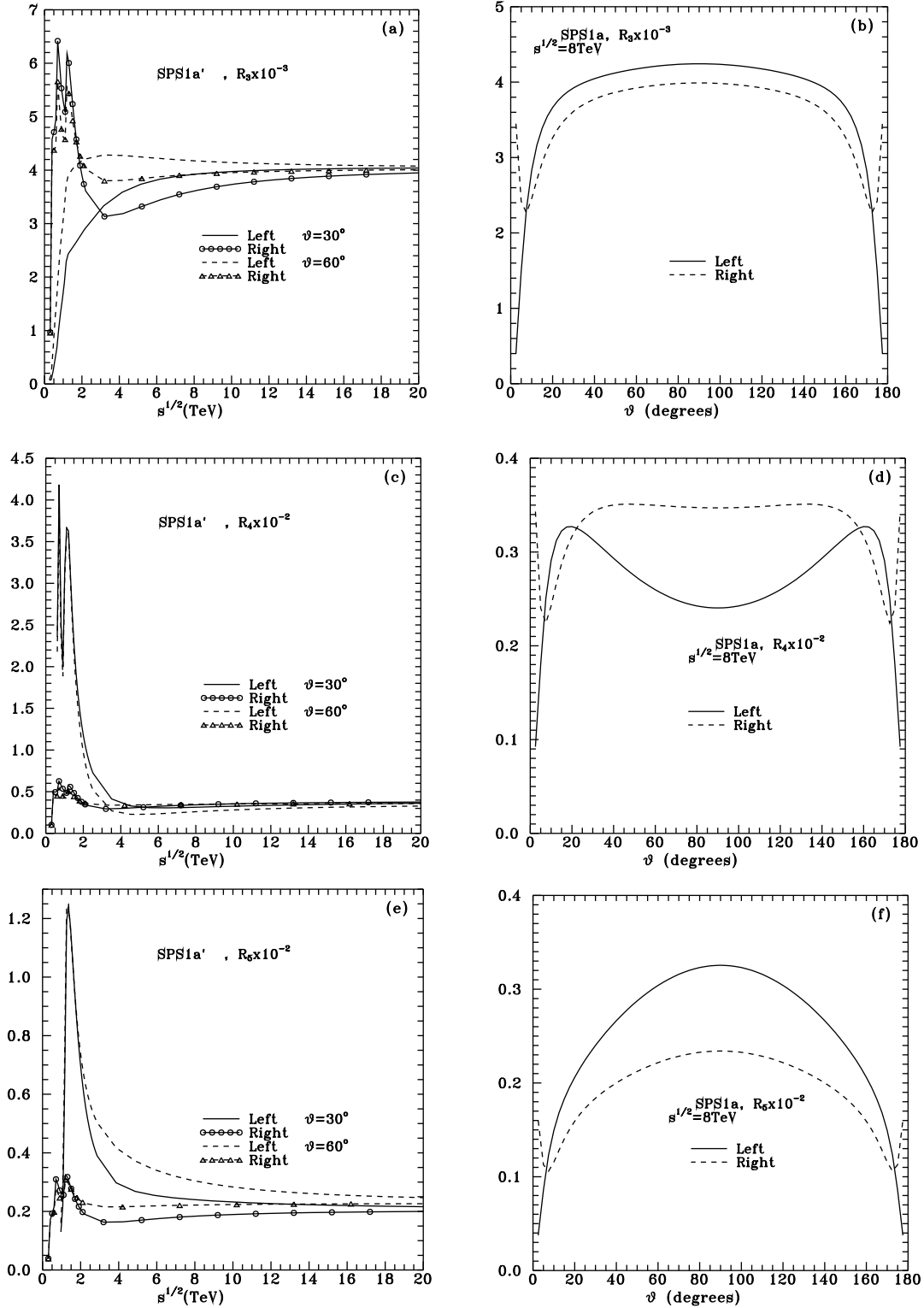


Figure 13: Magnitudes of the Left and Right parts of the asymptotic relation R_3 , R_4 , R_5 defined in (25, 26, 27); (a,c,e) describe the energy dependencies, while (b,d, f) give the angular dependencies at $\sqrt{s} = 8$ TeV.

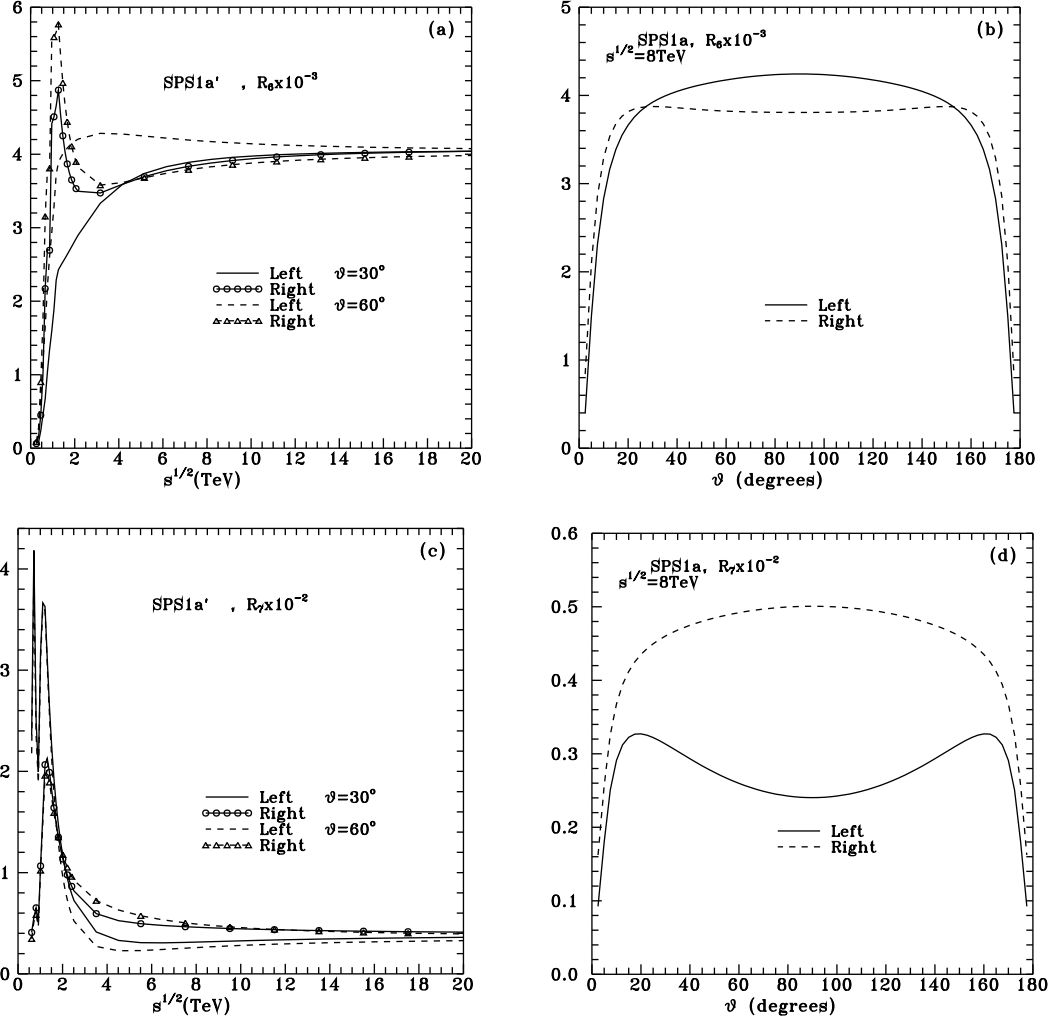


Figure 14: Magnitudes of the Left and Right parts of the asymptotic relation R_6 , R_7 , defined in (29, 30); (a,c) describe the energy dependencies, while (b,d) give the angular dependencies at $\sqrt{s} = 8$ TeV.